

2018

Acousto-Ultrasonic SHM/NDE Methods Toward Field Application

Stephen Harris Howden
University of South Carolina

Follow this and additional works at: <https://scholarcommons.sc.edu/etd>



Part of the [Mechanical Engineering Commons](#)

Recommended Citation

Howden, S. H.(2018). *Acousto-Ultrasonic SHM/NDE Methods Toward Field Application*. (Master's thesis). Retrieved from <https://scholarcommons.sc.edu/etd/4904>

This Open Access Thesis is brought to you by Scholar Commons. It has been accepted for inclusion in Theses and Dissertations by an authorized administrator of Scholar Commons. For more information, please contact digres@mailbox.sc.edu.

ACOUSTO-ULTRASONIC SHM/NDE METHODS TOWARD FIELD APPLICATION

by

Stephen Harris Howden

Bachelor of Science
University of South Carolina, 2015

Submitted in Partial Fulfillment of the Requirements

For the Degree of Master of Science in

Mechanical Engineering

College of Engineering and Computing

University of South Carolina

2018

Accepted by:

Lingyu Yu, Director of Thesis

Victor Giurgiutiu, Reader

Cheryl L. Addy, Vice Provost and Dean of the Graduate School

© Copyright by Stephen Harris Howden, 2018
All Rights Reserved.

ACKNOWLEDGEMENTS

I want to express my thanks to all who helped me along the way. I want to thank Dr. Lingyu Yu for her guidance as my advisor, Dr. Victor Giurgiutiu for his teaching and instruction, my fellow colleagues for their input, help, and unusual foods, and my family for their support.

ABSTRACT

Acousto-ultrasonic nondestructive evaluation (NDE) and structural health monitoring (SHM) methods offers solutions in damage detection, material properties evaluation and more. These ultrasonic waves can propagate through solids and interact with structural features and discontinuities. In this thesis use of several acousto-ultrasonics NDE/SHM methods were explored to evaluate their sensing and detection capabilities toward damage detection field applications in nuclear and aerospace industries.

For nuclear applications, passive sensing using piezoelectric sensors and acoustic emission (AE) techniques were explored on the spent fuel dry storage casks. Dry storage casks are used in the nuclear industry to transport or store spent nuclear fuel over long periods. NDE and SHM of these structures during their extended usage is highly desired to determine integrity and health of these components. Ultrasonic NDE/SHM potentially offers a solution as they can penetrate such structures and interact with the damage for timely detection if it presents. In this thesis ultrasonic guided waves excited by passive and active means are studied with the goal of determining the feasibility of such methods toward application on actual dry storage casks. Extensive experimental studies have been conducted on small, medium, and large-scale cask structures or similar.

For aerospace applications, as aircraft technology progresses so does the number of composites used in aerospace construction. Hence, a means of nondestructive

inspection is also desired. Within this thesis bond quality with various defects or contaminations were targeted and explored with both contact and non-contact type ultrasonic sensing methods. The contact methods are well established but require the use of additional coupling materials; while the non-contact means remove such a need and could lead to quick inspections but need further study to confirm their NDE/SHM capability. Results from both types were obtained and compared to the current standard techniques for evaluation and validation.

PREFACE

Partial material is based upon work supported by NASA under Award Nos. NNL09AA00A and 80LARC17C0004. Any opinions, findings, and conclusions or recommendations expressed in this material are those of the author and do not necessarily reflect the views of the National Aeronautics and Space Administration.

TABLE OF CONTENTS

Acknowledgements.....	iii
Abstract.....	iv
Preface.....	vi
List of tables.....	ix
List of figures.....	x
List of abbreviations	xiv
CHAPTER 1 Introduction.....	1
CHAPTER 2 State of The Arts	3
2.1 Ultrasonic nondestructive evaluation (NDE).....	3
2.2 Guided waves transducers and excitation	4
2.3 Acoustic emission method	7
2.4 SHM for nuclear dry storage cask.....	7
2.5 SHM/NDE for bonded aero structures	9
CHAPTER 3 Passive acoustic emission for dry storage Cask shm/nde	12
3.1 Problem definition and work scope.....	12
3.2 Medium-scale AE study.....	13
3.3 Small-scale AE study	19
3.4 Full-scale AE tests.....	27

3.5	Additional active sensing	33
3.6	Conclusions	34
CHAPTER 4 Bond quality detection		36
4.1	Introduction of bond layer contamination in composites.....	36
4.2	Specimen preparation.....	37
4.3	Impedance method	43
4.4	Immersion tank C-Scan	46
4.5	Non-contact scanning systems	49
4.6	Problems encountered	56
4.7	Preliminary studies.....	57
4.8	Conclusions	60
CHAPTER 5 Conclusions.....		64
References.....		67

LIST OF TABLES

Table 3.1: Sensors, excitation type, and impact locations	16
Table 3.2: Passive AE sensor and excitation locations	22
Table 3.3: PWAS receiving and excitation locations	22
Table 3.4: Acquisition setup within AEWin for Experiment 1 where sensors A, B, C, and D were represented as 1, 2, 3, and 4 respectively	29
Table 3.5: Localization setup for Experiment 1	30
Table 4.1: Bonded specimens made and their characteristics with approximate warming time	38
Table 4.2: Recipe 1 used for all specimen bonding	39
Table 4.3: Scan parameters	53
Table 4.4: Systems used and abilities to detect bond layer damages in specimens tested	63

LIST OF FIGURES

Figure 2.1: Waves propagating in aluminum plate	4
Figure 2.2: Various sensing methods with a) PWAS, b) LDV, c) PL, d) ACT	6
Figure 2.3: Overview of a typical passive AE system	7
Figure 2.4: Holtec HI-STAR dry storage cask a) cross-section [13] and b) in vertical storage [14]	8
Figure 2.5: Boeing 787 Dreamliners with material makeup [23]	10
Figure 3.1: Nuclear vacuum chamber structure with a) labels and close-look of sensor sets on b) F1 and c) S1 [29]	14
Figure 3.2: (a) Stainless steel impact hammer with (b) assembled tip [30] [29]	14
Figure 3.3: Pictures of an a) 2/4/6 preamplifier and the b) digital AE system	15
Figure 3.4: Sensing range of structure from the farthest points using stainless steel tipped banging and PLB excitation methods [29].....	17
Figure 3.5: AE waveforms after passing through various structural conditions [29].....	18
Figure 3.6: Small-scale dry storage cask with a) lid on and b) off	19
Figure 3.7: Custom tip to be fitted on hammer	20
Figure 3.8: Sensors used experiments: a) WS α , b) R15 α , and c) PWAS wafers indicated with arrows.....	20
Figure 3.9: Shows the frequency domain of various excitation methods and sensor combinations	24
Figure 3.10: PLB and T304 tip impact hammer localizations of SG series using R15 α ..	25

Figure 3.11: PLB and T304 tip impact hammer localizations of SG series using WSa...	26
Figure 3.12: Impact locations on the front face consisting of the “a” series of excitation locations [30]	28
Figure 3.13: Impact hammer tip used for all experiments in inches [30]	29
Figure 3.14: Sensor placement view for Experiment 1 [30]	29
Figure 3.15: Sensors moved to a) trunnions A, B, C, D with b) a close-up image of a bonded sensor on trunnion C [30]	30
Figure 3.16: Layup of “b” series of excitation locations [30]	31
Figure 3.17: Series “a” detected impacts along with the actual locations [30]	32
Figure 3.18: Series “b” of simulated AE locations and true locations [30]	32
Figure 3.19: Small-scale max amplitude response measured from basket guides	33
Figure 3.20: Full-scale max amplitude response with excitation frequency ± 6 kHz excitation error where the channels correspond with the trunnions [30]	34
Figure 4.1: Plate damage layout from Specimens 1,2,4, and 5 from a) top down view and b) layup view	40
Figure 4.2: Process of weak bonding a) before application of contaminates and b) after drying for a composite specimen	41
Figure 4.3: Adhesive film applied to non-contaminated side and being cut	41
Figure 4.4: Damage preparation of Specimen 3 with a) prepared bagging tape sections to be inserted in and b) plate with adhesive applied where a section is removed to create a void	43
Figure 4.5: Specimen 3 a) damage layout and b) layup were locations of bagging film can be seen	43
Figure 4.6: Plate 2 with a) sensors attached and b) layout of sensors	44

Figure 4.7: Sample data from Point 1 of a) first peak resonance and b) through thickness resonance..... 45

Figure 4.8: Max impedance resonance and their corresponding frequencies at a) first peak and b) through thickness peaks 46

Figure 4.9: Immersion tank used for ultrasonic C-scan inspection 46

Figure 4.10: Immersion tank scan of Specimen 2 using a 10 MHz focused transducer using pulse echo single penetration displaying APA of signal between 1.235 to 1.285 μ s..... 48

Figure 4.11: Immersion tank scan of Specimen 5 using a 10 MHz focused transducer pulse echo single penetration displaying APA of signal between 1.73 to 1.78 μ s with closeup of 3 \times 3 inch area of selected damaged area 49

Figure 4.12: Simple block diagram of the system 50

Figure 4.13: The scanning system a) equipped with ACT-LDV, b) ACT-ACT and c) diagram of sensor alignment..... 51

Figure 4.14: Scan areas on Specimen 3 53

Figure 4.15: Location 1 APA scan area detecting a 0.5 by 0.5 inch bagging film using a) ACT-ACT at 120 kHz Settings 1 b) ACT-ACT at 225 kHz c) ACT-ACT at 400 kHz d) ACT-LDV at 225 kHz where the red box indicates the disbond size and location 54

Figure 4.16: Location 4 APA scan area detecting a roughly 3.25 by 0.25 inch section of bagging film using a) ACT-ACT at 120 kHz b) ACT-ACT at 225 kHz c) ACT-ACT at 400 kHz..... 55

Figure 4.17: ACT-ACT 120, 225, and 400 kHz 2 \times APA a) scan areas and b) scans 56

Figure 4.18: Dummy pulse laser a) flange and b) mounted on a KUKA KR6..... 58

Figure 4.19: Function box with oscilloscope resting on top showing the output signal... 59

Figure 4.20: Alignment tools with a) line laser housings and b) target for calibration 60

Figure 4.21: Immersion tank scan of Specimen 4 APA between 1.575 and 1.625 μ s at with closeup of ACT-ACT 400 kHz scan APA between 300 and 301 μ s..... 62

Figure 4.22: ACT-ACT 2×2 inch through transmission APA 50 to 100 μs C-Scan of damage on Specimen 4 of damaged region with 3×3 inch immersion scan contour overlap using a) 120 kHz b) 225 kHz and c) 400 kHz transducers 62

LIST OF ABBREVIATIONS

AE	Acoustic emission
ACT.....	Air coupled transducers
APA.....	Absolute peak amplitude
EMI	Electromechanical impedance
FBG.....	Fiber Bragg grating
LBI	Laser bond inspection
LDV	Laser Doppler vibrometer
NDE	Non-destructive evaluation
PL.....	Pulse laser
PLB	Pencil lead break
PWAS	Piezoelectric wafer active sensor
SHM.....	Structural health monitoring
SLDV	Scanning laser Doppler vibrometer
SNF	Spent nuclear fuel

CHAPTER 1 INTRODUCTION

On April 28, 1988 Aloha Airlines Flight 243 suffered a midflight explosion that resulted in one fatality [1] [2]. After landing, the source of the explosion was the determined to be the result of fatigue cracking along the rivets of the fuselage [2]. As civilization continues to grow and more complex devices that transport, hold, shelter and aid in society are created, has pushed the demand to insure the safety those structures as well as to provide guidance for maintenance. Accidents such as Flight 243 serve as late reminders of the lack or shortcomings of means to prevent such disasters from occurring. Structural health monitoring (SHM) is needed for the continuous observation of the wellbeing of essential parts. Providing nondestructive SHM gives the additional benefit of not damaging the part, yet potentially offering a more cost-effective solution.

Each industry and component provides its own set of challenges for implementing SHM. Shelled or plate-like structures offer the means for ultrasonic waves to propagate [3]. These waves have been known as guided waves and of great interest due to their effectiveness in the identification of structural damage. Their long propagating abilities and sensitivity to differences in the media in which they travel fuels interest in using such methods in solving real world needs.

Within this thesis, passive and active sensing techniques using guided waves are therefore explored on real-world applications including SHM for nuclear spent fuel dry storage casks and aero structure bonding quality evaluation. Various sensing techniques are studied using contact, non-contact, or hybrid actuators/sensors in determining passive

and active sensing capabilities on these real-world applications toward pushing SHM methodologies for field applications.

CHAPTER 2 STATE OF THE ARTS

Contained within this paper is a board range of literature study exploring the current state of the arts of related sensing methods for the selected nuclear or aerospace applications.

2.1 Ultrasonic nondestructive evaluation (NDE)

Similarly to dropping a rock in a pond and watching the ripples, waves will propagate within solid median (Figure 2.1). Like with ripples interacting with nearby rocks, once ultrasonic waves come across a dissimilar material or material discontinuity the propagating waves will be disrupted causing reflections, mode conversions, and more [3]. Ultrasonic testing is one of the most established nondestructive evaluation (NDE) methods used in practice due to its high sensitivity and abilities to detect both surface and internal defects [3]. There are often two basic configurations used in ultrasonic wave based SHM, pulse-echo and pitch-catch methods. The pulse-echo method uses a single side/location of excitation and sensing [3]. Ultrasonic waves propagate from one location and the echo/reflected waves are received at the same point or transducer. Pitch-catch method operates with a point of excitation and at a secondary location where the elastic waves are detected. These two different configurations are generally common with most types of transducers.

Typical ultrasonic NDE testing is conducted in a tank full of water, namely the immersion tank method. The specimen under inspection is submerged and a probe is

lowered into water. The probe, or probes, through either pitch-catch or pulse-echo configurations will excited pressure waves which will pass through the water, specimen, back through the water, and is received. The water coupling improves sensitivity and efficiency when compared to air-coupled transducers. However, the specimen and supporting transducers must be exposed to water. Overall immersion tank inspection is the conventional method used in industry to identify product defects.

2.2 Guided waves transducers and excitation

With the ability of propagating over a large area within the upper and lower surfaces and sensitivity to various abnormalities, ultrasonic guided wave based damage identification offer many advantages over traditional ultrasonic testing [3, 4].

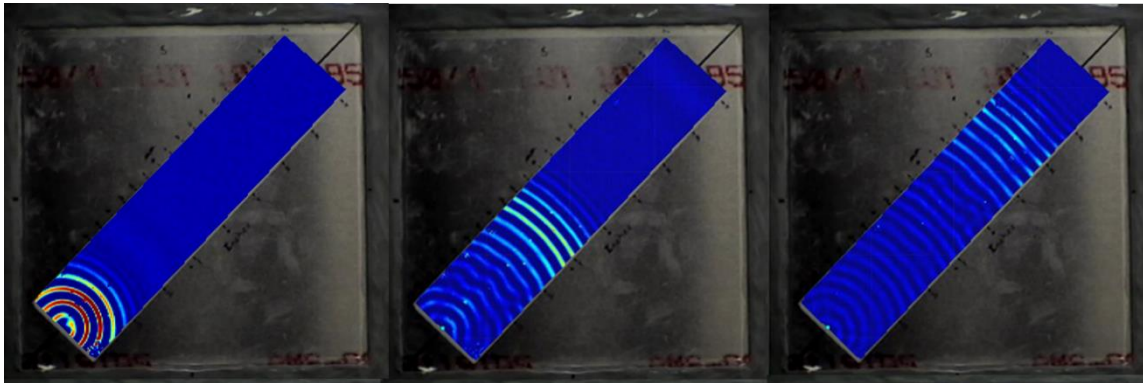


Figure 2.1: Waves propagating in aluminum plate

To create a measurable disturbance within the media for guided wave SHM, various transducers have been developed. One of the reliable and inexpensive ways is to use wafer type piezoelectric material and bond it to the structural surface using adhesives (Figure 2.2a). These transducers are often referred to as piezoelectric wafer active wafer (PWAS) [4]. When strain occurs within the PWAS material, it produces an electrical voltage. This allows for direct translation of the mechanical energy in the propagating waves to an electrical signal that can be measured [4]. In addition, when applying

alternating voltage to a PWAS, it will create strain within the piezoelectric material. If bonded to a surface, this will thereby introduce strain into the structure. PWAS are considered a contact method as they need to be bonded to the surface of the structures for inspection. Depending on the structure, bonding could be problematic. Bonding sensors also requires surface preparation and long-term maintenance. Depending on the number of sensors, all these can be tedious and time consuming which restricts field application.

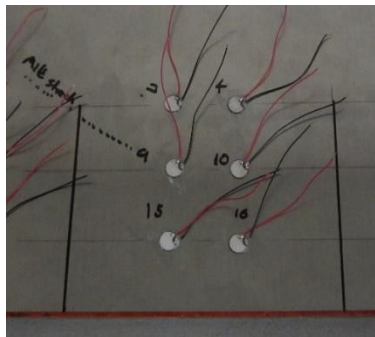
Air coupled transducers (ACT) work on the same piezoelectric principle as PWAS but using air as the coupling with the structure. They usually have lower sensitivity compared to either PWAS or traditional ultrasonic testing methods, however provide fully non-contact sensing capabilities (Figure 2.2b). The advantages include eliminating solid or liquid coupling as well as supporting accessories such as pumps, filters, and other hardware [5]. For the system to operate with air as a coupling, a built-in amplifier is needed to create a sufficient disturbance to excite ultrasonic waves within the specimen. The ACT can operate in pulse-echo configuration where a receiving ACT is needed or other guided waves sensing as in a hybrid system. The receiving ACT transducer also requires additional amplification and other settings to properly obtain a satisfactory waveform.

A laser Doppler vibrometer (LDV) is another non-contact guided wave sensing device. The LDV allows for waves to be measured from a distance. It shines a laser onto the specimen and based upon the light's change in frequency via the Doppler effect, can estimate the specimen's surface velocity normal to the laser [6]. Some models of such devices contain scanning capabilities and are known as scanning LDV (SLDV).

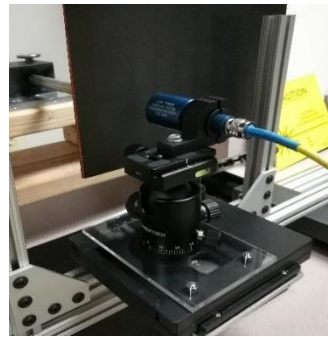
Downsides to the LDV or SLDV acquisition system is that any obstruction of the beam

will result in a lost signal. Meaning that a direct line of sight is required without special instrumentation. Also, the reflectivity of the surface of the specimen being inspected is vital as non-reflective surface conditions will result in poor or no signal. This limits the sensing capabilities and/or requires surface preparation for acquisition.

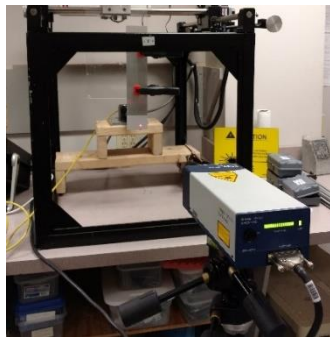
Non-contact means of guided wave actuation can be achieved with pulsed laser (PL) excitation method. PL uses the energy from projected light to create elastic waves via thermal expansion [7]. Drawbacks with PL excitation are that a relatively powerful laser is required (Figure 2.2d) and damage to the surface of the test structures can occur due to burning or ablation. Cooling for such a device is also critical as well as supporting pumps, shielding, and extra equipment.



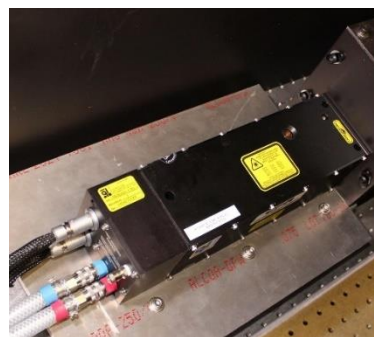
a)



b)



c)



d)

Figure 2.2: Various sensing methods with a) PWAS, b) LDV, c) PL, d) ACT

2.3 Acoustic emission method

Crack growth within a material causes a release of strain energy [8], known as acoustic emission (AE). The mechanism of which is described within fracture mechanics [9]. AE sensing relies on this mechanism of energy release to trigger acquisition (Figure 2.3), and therefore is a passive system [3, 9]. Sensors designed for detecting this release of energy are specifically manufactured for this task. Some are designed to have resonance at a select frequency, meaning that is a small periodic force, such as a passing wave, can drive large amplitude oscillations [10]. To aid in the acquisition, supporting computers and amplifiers are generally used.

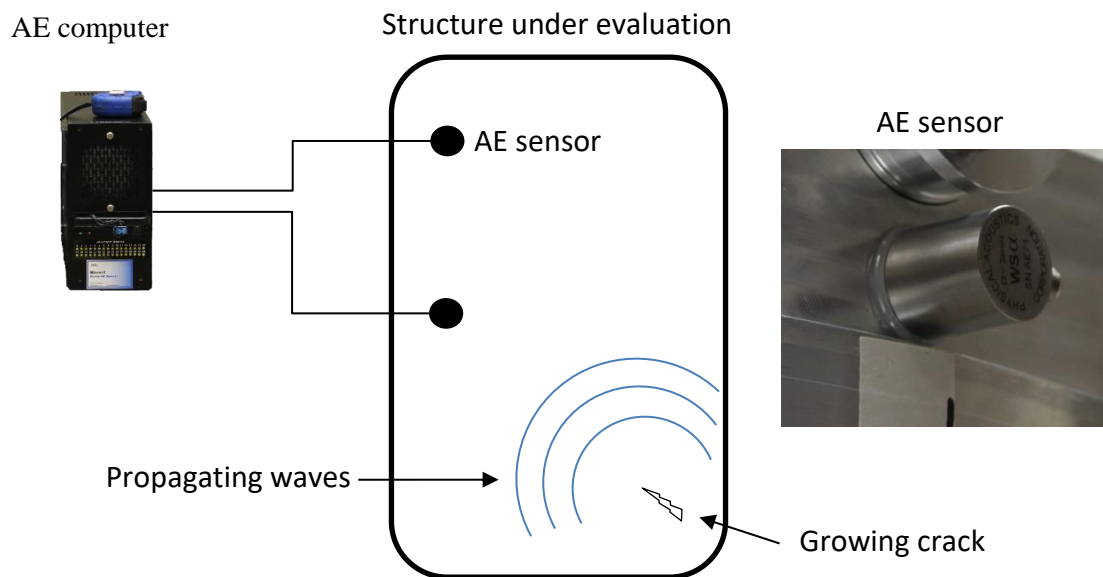


Figure 2.3: Overview of a typical passive AE system

2.4 SHM for nuclear dry storage cask

Since the start of nuclear energy production, over 130 nuclear power plants have been built within the U.S. As stated by the United States Nuclear Regulatory Commission, "...late 1970s and early 1980s, the need for alternative storage began to

grow when pools at many nuclear reactors began to fill up with stored spent fuel. Utilities began looking at options such as dry storage cask for increasing spent fuel storage capacity [11]”. The purpose of these casks is to protect personnel and the environment by allowing the spent nuclear fuel (SNF) to cool during their decay without leakage and to provide radioactive shielding of the waste [12]. These dry storage casks are generally cylindrical structures where they are either bolted or welded closed after SNF is added. To prevent leakage of the hazardous waste there are multiple shell-like fixtures inside. For gamma radiation shielding, steel, concrete, and lead are generally used. Additional layers of polyethylene, boron-impregnated material or more concrete is used for neutron shielding [12]. A cross-section of one model of these devices is shown in Figure 2.4.

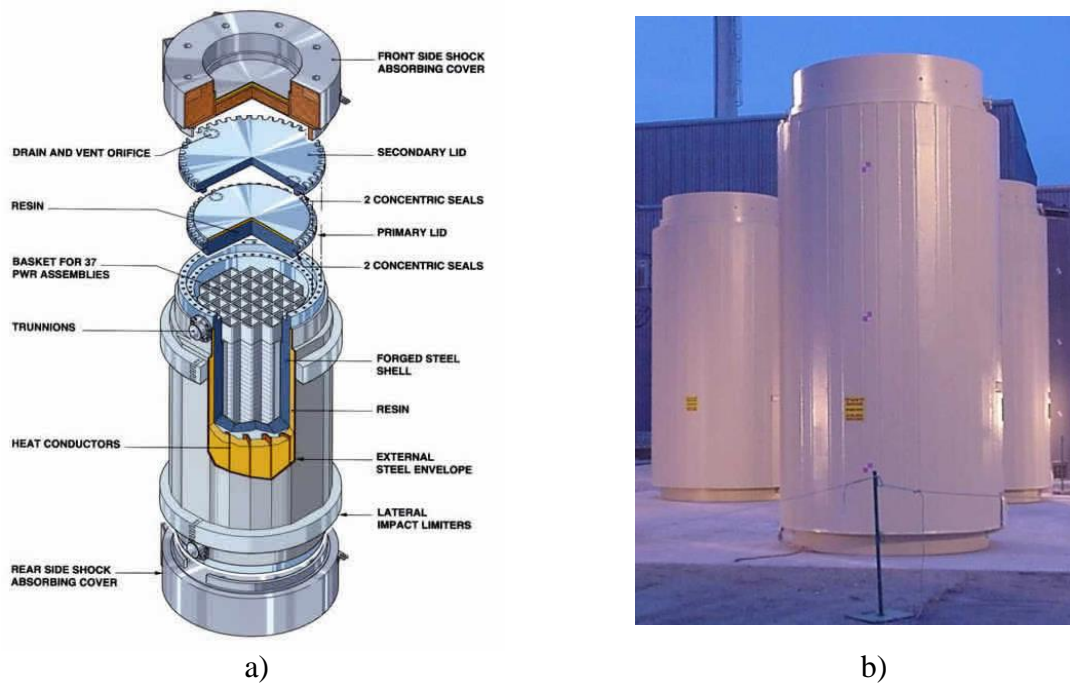


Figure 2.4: Holtec HI-STAR dry storage cask a) cross-section [13] and b) in vertical storage [14]

As of 2016 the DOE reported that 204 bare fuel and 2073 canister fuel casks are in use in various cask models available. This makes up a total of 92,511 used fuel assemblies in storage casks [15]. With a vast amount of fuel in dry storage cask and the continued licensing of the aging containers continuing, concern has risen that the hazardous radioactive waste could result in cracking [16, 17]. Thus, many sensing methods and techniques have and are undergoing evaluation [18]. All the sensing methods being reviewed have their strengths and weaknesses. Some of the current methods under evaluation include a robotic delivery system for laser-induced breakdown spectroscopy (LIBS) and noncontact electromagnetic acoustic transducers (EMATs) for inspection [19] [20]. The dual delivery will allow the LIBS to detect salt deposits on the canisters surface while the EMATs will detect the cracks [19]. However, the system is still under development as the robot will need to maneuver the ventilation and interior while collecting data [19]. Also, this system will not be capable of continuous monitoring.

A more abstract means of inspection is the use of muons (cosmic rays) in determining damage [16, 21]. Muon imaging operates by detecting the energy loss and reflections from inelastic collisions with electrons [17]. Simulations have shown that missing rods could be detected in vertical detection cases, but not in the horizontal cases [21]. Drawbacks of such a system include specialized equipment, periods of time needed for acceptable resolution, and the inability to detect instantaneous crack growth.

2.5 SHM/NDE for bonded aero structures

Composite structures offer many advantages over traditional aluminum construction in aerospace construction. They are lighter, superior at absorbing vibrations,

and yet are still flexible and strong [22]. Half of the materials used in the Boeing 787 (Figure 2.5) are advanced composites offering a 20% reduction of weight compared its aluminum counterparts [23].

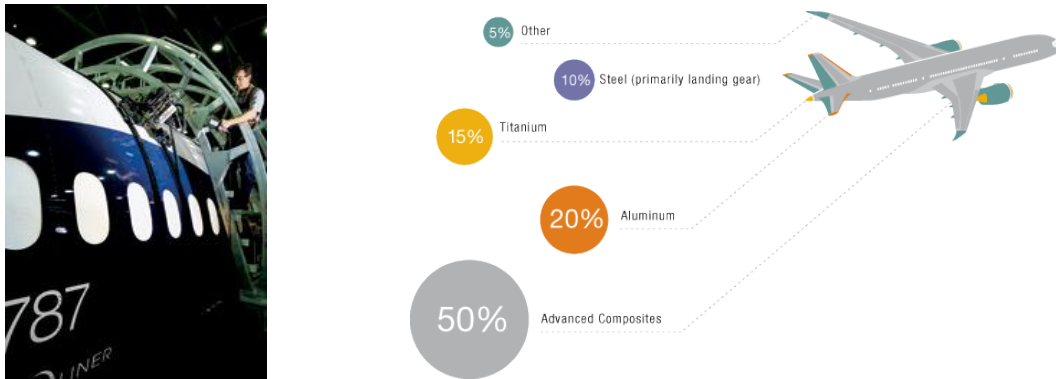


Figure 2.5: Boeing 787 Dreamliners with material makeup [23]

Traditionally, aluminum structures were riveted together requiring holes to be drilled. This was time consuming and created regions of stress concentration which overtime has resulted in failure, such as in Aloha Airlines Flight 243 [2]. Not only are drilling holes undesirable but due to the carbon fiber within composites, holes would significantly reduce their load bearing properties. Thus, adhesive bonding is desired as it has more uniform stress distribution and the ability to combine dissimilar materials [24].

With the addition of composites and adhesive bonding comes the possibility of contamination occurring during the process. Previous studies have shown that detecting this contamination can be difficult [25]. Many methods are being investigated such as laser bond inspection (LBI) and electromechanical impedance (EMI) method [25].

LBI operates by firing a sequence of three laser pulses in a low-high-low manner. The first low pulse is used to record a baseline measurement. Following the low pulse, a high energy pulse is fired. If a weak bond is present at the point of laser contact, the bond

will fail. The final low pass pulse is recorded and compared to first low energy pass. If the signals are identical then the bonding at that point is considered strong [25, 26, 27]. LBI is considered a NDE method as no damage is generated to strong bonds, however, structural engineers are reluctant to adopt this method because of the high costs, limitations of data, and the possibility of creating damage [25]. Also, the setup requires preparation which can include tape and an O-ring to hold water, limiting the system's functionality [27].

Research using EMI has been shown to be effective in detecting bond layer contamination [28]. This was accomplished by bonding piezoelectric wafers to the surface of the specimen. The identification of various admittance peaks was used in characterizing contamination trends [28]. However, this method required contact with the surface of the structure under evaluation and is still undergoing investigation.

CHAPTER 3 PASSIVE ACOUSTIC EMISSION FOR DRY STORAGE CASK SHM/NDE

3.1 Problem definition and work scope

Many of the nuclear dry storage cask facilities are located near the coast where salt is present in the air. This along with their extended periods of use [16] has created concern that these casks could develop damage over time and has driven the need for NDE and SHM [8].

However dry storage cask inspection faces many difficult challenges for NDE/SHM of the conditions. First, the lid cannot be removed because of the radioactive hazards. Second, access for visual inspection of the components is limited to the vents, which is difficult for even modern robots and limits inspection to the outside shell surrounding the basket [20]. Though certain other technical methods exist; each has its own strengths and weaknesses [18].

As discussed in Chapter 2, ultrasonic NDE offers the potential for relatively affordable and effective sensing [3, 4] detecting instantaneous damage growth [9], and the possibility for external sensing for internal defects. However, to apply ultrasonic NDE/SHM for dry storage casks, challenges still exist including sensing through the thick cask walls and determining the features of the signals that can indicate damage. Overall the complexity, size, wall thickness, access points and varying materials pertinent to the dry cask structures create many challenges for using guided waves based

NDE/SHM [18]. Little is known about the ultrasonic experimental sensing capabilities on dry storage casks.

Hence this chapter focuses on passive acoustic emission (AE) methods for nuclear dry storage cask NDE/SHM. The chapter first examined the sensing capabilities on a medium-scale vacuum chamber structure available at USC [29] to evaluate the range and sensing capabilities of AE methods. The study then progressed to a small-scale mockup cask. After these, full-scale field experiments were conducted where passive localization techniques and active testing were performed and analyzed.

3.2 Medium-scale AE study

A medium-scale experiment was first performed to explore the sensing capabilities of AE techniques on complex structures using a vacuum drying chamber available at USC. An impact hammer with various tips along with pencil lead breaks (PLB) were used to simulate AE events. A wide range of locations were tested to evaluate AE sensing range, capabilities and structural influences.

3.2.1 Experimental setup

The vacuum drying chamber was divided into sections and labeled where areas of sensing and excitation could be identified (Figure 3.1a) [30]. To monitor the AE events, six AE sensors in two sets of three were applied using hot glue (as it was easily removable and resulted in no damage) to the surface of the chamber. Each set contained one of each Physical Acoustics R15I, R15 α , and a WS α AE sensor¹ for Round 1. Later a R15 α and a WS α were used to measure the maximum range as they performed the best in

¹ <http://www.physicalacoustics.com/sensors/>

Round 2. All AE signals were collected using Physical Acoustics MICRO II Digital AE system (Figure 3.3b). A PCB model 086C04 impact hammer² with a built-in accelerometer and a PLB with 0.07mm lead were used to excite the AE signals. Two hammer tips were used for testing: a plastic PCB tip and a custom made 304 stainless steel tip (Figure 3.2). To boost the signals Physical Acoustics 2/4/6 preamplifiers³ (Figure 3.3a) operating at 40 dB were used on the AE sensors except for the R15i sensor which already has an integrated amplifier.

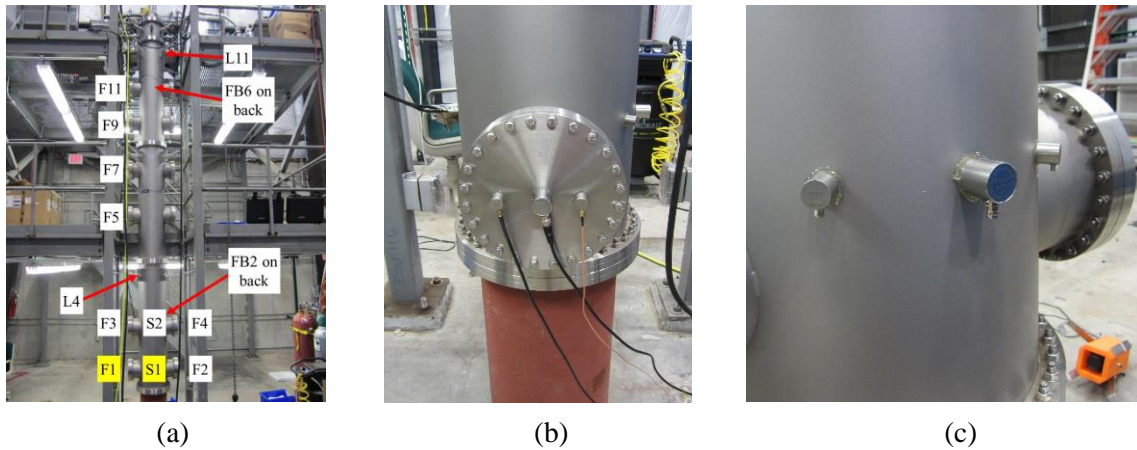


Figure 3.1: Nuclear vacuum chamber structure with a) labels and close-look of sensor sets on b) F1 and c) S1 [29]



Figure 3.2: (a) Stainless steel impact hammer with (b) assembled tip [30] [29]

² <http://www.pcb.com/TestMeasurement/ImpactHammers>

³ <http://www.physicalacoustics.com/by-product/2-4-6/>



a)



b)

Figure 3.3: Pictures of an a) 2/4/6 preamplifier and the b) digital AE system

3.2.2 AE sensing procedure

For each set of sensor location, PLB, stainless steel tip impact hammer, and plastic tip impact hammer excitation were implemented. For each set tests were executed for three times to ensure consistent results. Three additional tests were taken for each point for a combined nine hits per checked location.

A second round was performed but with PLB only. Extra effort was used to ensure precise PLB events. Also, only the WS α and the R15 α were used since it was found R15i transducers provided weaker signals in the first round of testing. Two runs were made where the sensors were exchanged. The first run used with just two WS α sensors and the second with two R15 α sensors where one sensor was bonded on F1 and the second in the center of S1. The overall test scheme was summarized and listed in Table 3.1.

Table 3.1: Sensors, excitation type, and impact locations

Round 1																
Sensing Location	Excitation	Excitation Location														
		F2	F3	F4	F5	F7	F9	F11	FB2	FB6	L4	L11	L12	S2	SB2	SB4
F1	PLB	✓	✓	✓					✓		✓			✓		
	Stainless steel tip	✓	✓	✓	✓		✓	✓	✓	✓	✓	✓		✓		
	Plastic tip	✓	✓	✓					✓		✓			✓		
S1	PLB		✓						✓		✓			✓		
	Stainless steel tip		✓		✓	✓		✓	✓	✓	✓	✓		✓		
	Plastic tip		✓						✓		✓			✓		
Round 2																
F1	PLB		✓			✓					✓		✓	✓	✓	✓
S1	PLB		✓			✓					✓		✓	✓	✓	✓

3.2.3 Results

First examined was the AE maximum sensing distance (L11 or L12 to F1) in the complex structure. From the top of the structure, impacts from the stainless-steel tipped impact hammer banging was detected as well as the PLB with the WS α and R15 α sensors (Figure 3.4). The steel tip hammer excitation resulted in lower frequencies signals compared to those by the PLB excitation. Also, the PLB produced a much higher amplitudes and more defined frequency peaks.

Among the three AE sensors, the R15i was the most difficult to trigger. The signals often blended in with the background noise. On the other hand, the sensors with external amplifiers, WS α and R15 α produced better signals and were to be used again in the analysis of Round 2.

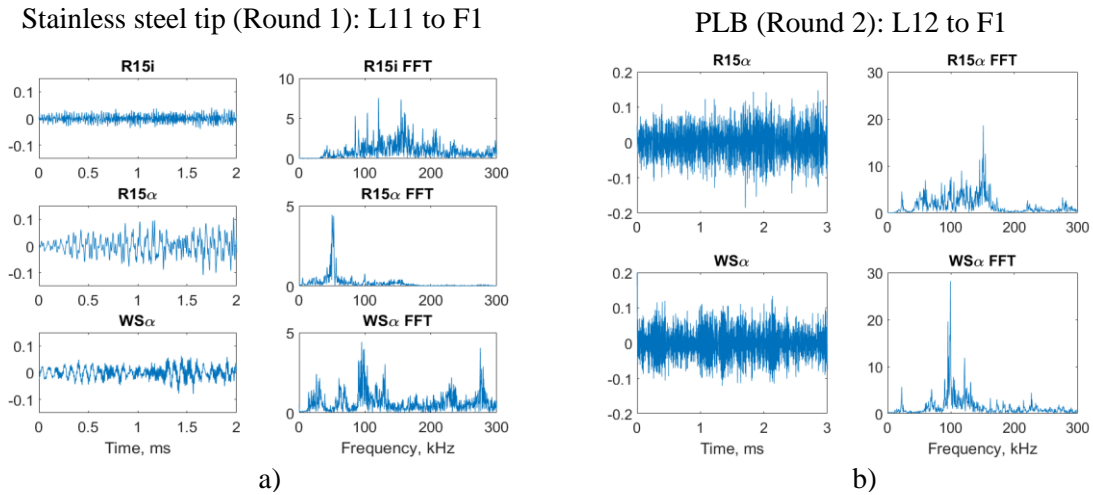
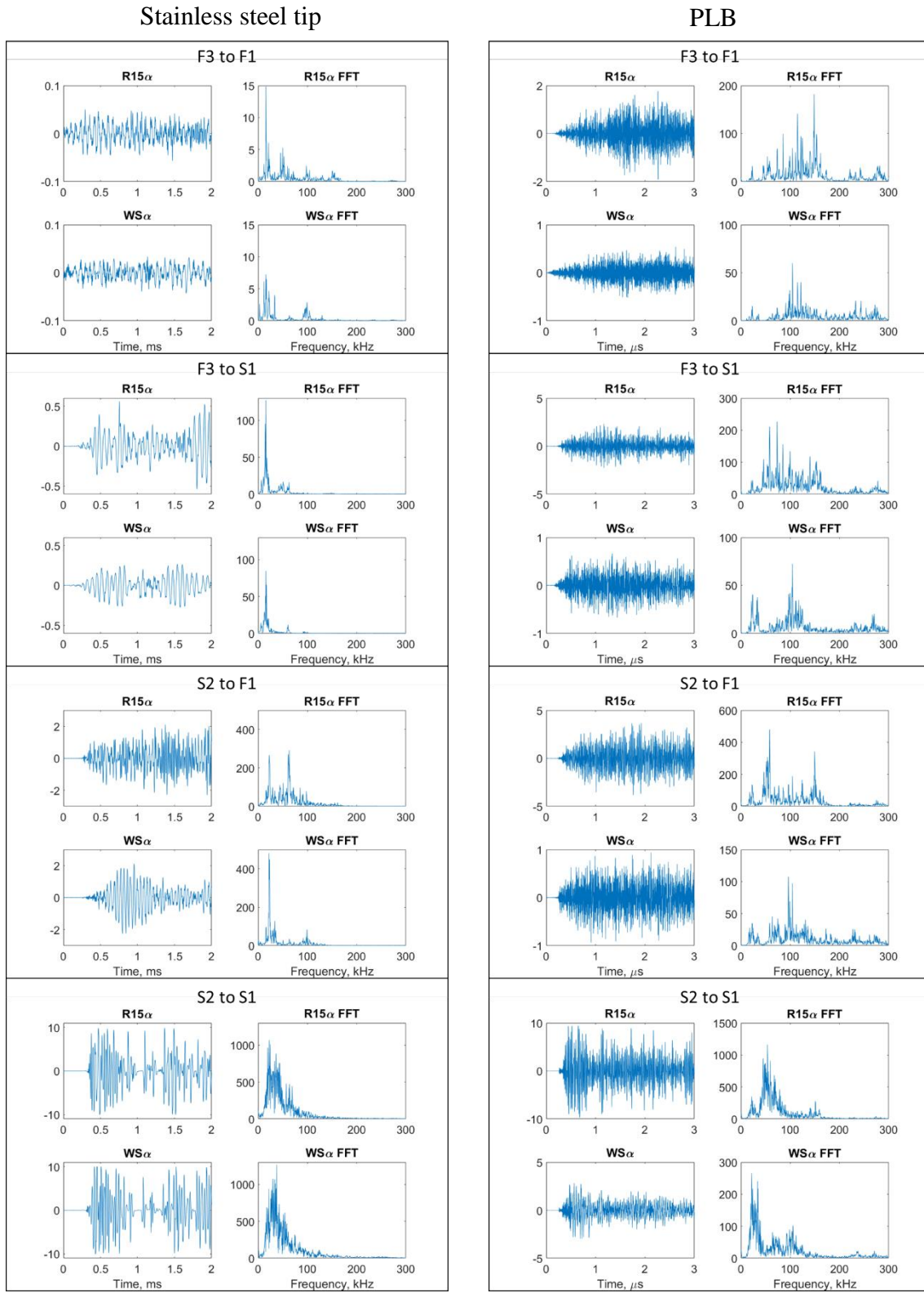


Figure 3.4: Sensing range of structure from the farthest points using stainless steel tipped banging and PLB excitation methods [29]

Next investigated was the structural influence on the signals. Examining the stainless-steel impacting and the PLB excitation methods showed changes that the flange and surface combinations produced (Figure 3.5). The structural complexity influence on the AE sensing for various cases of structural characteristics are as follows: surface to surface (S2 to S1), surface to flange (S2 to F1), flange to surface (F3 to S1), and flange to flange (F3 to F1). When examined, the stainless-steel impacting (Figure 3.5a) exhibited lower frequency components under 100 kHz. Closer observation of the frequency spectra showed changes in the locations of peaks. For the surface case the frequency plot (Figure 3.5, S2 to S1) showed a gradual increase to a single frequency for both WS α and R15 α sensors. However, when one or more flanges were introduced multiple and more defined peaks occurred. This was similar with the PLB excitation interaction with the flanges. In addition, examining the stainless-steel tip hammer impacting and the PLB excitation both methods showed changes that may be caused by the flange and surface combinations (Figure 3.5)



a) b)
 Figure 3.5: AE waveforms after passing through various structural conditions [29]

3.3 Small-scale AE study

The next phase was to employ the AE sensing techniques used on a small-scale dry storage cask (Figure 3.6). Active sensing with the same set up AE sensors being used will also be study in order to evaluate the sensor's potential for dual passive-active (i.e. acousto-ultrasonic) integrated NDE/SHM. The procedures and methods tested in this small-scale structure will later be applied in a similarly manner to the full-scaled dry storage cask field test to be discussed in later sections.

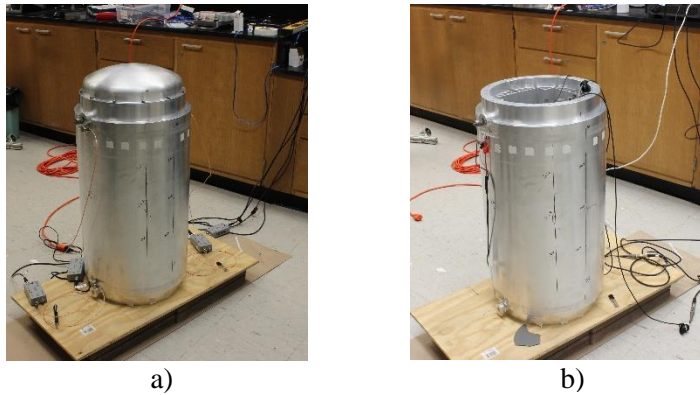


Figure 3.6: Small-scale dry storage cask with a) lid on and b) off

3.3.1 Experimental Setup

In order to choose appropriate excitation methods for sensing in the small-scale mockup, a variety of excitation techniques were used to examine the range of frequency responses.

3.3.1.1 Excitation methods

The same PCB Model 086C04 impact hammer from the previous medium-scale testing was used for excitation in AE tests, but fitted with a custom made T304 stainless steel tip (Figure 3.7). This tip was made from a signal piece of steel to prevent foreign material falling into the casks during impacting and was used for all impact hammer

excitations from now on for the small- and full-scale experiments. Standard PLBs were also used to excite relatively higher frequencies AE events within the mockup cask.

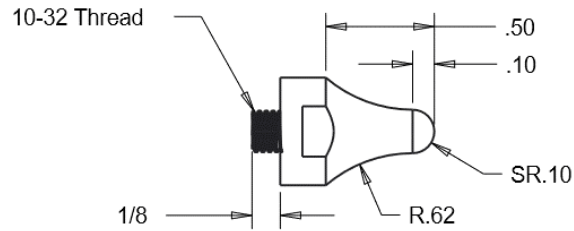


Figure 3.7: Custom tip to be fitted on hammer

New to the small-scale was the excitations by carbon steel balls of various sizes (0.25, 0.137, and 0.125 inch diameter) in order to excite a midrange response between the PLB and impact hammer. The balls were lightly thrown at the surface of the cast.

For the small-scale experiments three sensors were used: the PAC AE sensors WS α and R15 α , and PWAS wafers (Figure 3.8) made by Steminc with 7 mm diameter and 0.2 mm thickness. The wafers were bonded to the structure with M-Bond 200 strain gauge adhesive.

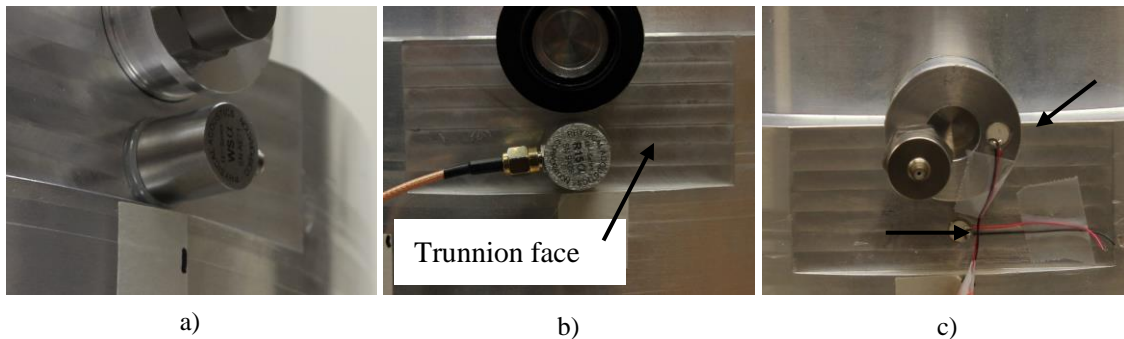


Figure 3.8: Sensors used experiments: a) WS α , b) R15 α , and c) PWAS wafers indicated with arrows

Before testing, sensor locations were selected on the mockup surfaces, trunnions, rims and basket guides. These locations were used for either excitation or sensor

placement. The placement of the sensors were selected such that passive and active sensing methods could be used to observe the structure's response to a variety of excitation combinations. The abbreviations for the locations are as follows:

- Trunnion: T series
- Trunnion face: TF series
- Grid of positions defined on front surface: SG series
- Arbitrary surface points: S series
- Point on inside lip of the rim: R series
- Basket guides: BG
- Inside basked: (no abbreviation)

For passive AE sensing, all the three sensors were used. Each time the sensors were in sets of four placed on the trunnion faces (Figure 3.8) except for the PWAS. The PWAS were small enough to be bonded to the trunnions and were also placed to the right portion of the trunnion (Figure 3.8c). In addition to sensor locations around, or on the trunnion. Additional PWAS wafers were also installed on basket inside the cask. For AE sensing using the PWAS wafers on the basket, a Tektronix TDS5034B oscilloscope was used to take advantage of averaging.

For active sensing the tests were aimed for detailed inspection of the frequency characteristics of specific cask features as the waves penetrated and passed through the surfaces. A Tektronix AFG3052C function generator was used along with a NF HSA 4014 amplifier to generate waves at 90 Vpp. The responses were recorded with the Tektronix TDS5034B oscilloscope.

3.3.2 Procedure

The testing began with the AE experimental configuration as given in Table 3.2 and Table 3.3. For some of the passive experiments, localizations were performed. The configuration tests intended to determine various parameters were needed for estimating

AE locations such as wave speed, event definition and etc. All the parameters were estimated by tuning after each replay. Once optimal settings were found the settings and impact locations were saved. Of these settings, the biggest influence of calculated AE localizations was found to be the estimated wave speed. All sets of data had the same wave speed and event definitions except for one point where the event definition was changed. The event definition had relatively insignificant influence on the calculated impact location. The active sensing with PWAS wafers consisted of linear sinusoidal sweeps and three count tone bursts excitations.

Table 3.2: Passive AE sensor and excitation locations

		T series				TF series				R series			S series			Basket	
		T1	T2	T3	T4	TF1	TF2	TF3	TF4	R1	R2	R3	S1	S2	S3	Top	
Basket in	AE wsa	P,I		P,I									P,I	P,I	P,I		
	AE R15a	P,I		P,I									P,I	P,I	P,I		
	AE PZT																
Basket out	AE wsa	P,I		P,I						I	I	I	I	I	I		
	AE R15a	P,I		P,I						I	I	I	P,I	P,I	P,I		
	AE PZT	P,I		P,I									P,I	P,I	P,I		

		SG series									BG series											
		SG1	SG2	SG3	SG4	SG5	SG6	SG7	SG8	SG9	BG1A	BG1B	BG2A	BG2B	BG3A	BG3B	BG4A	BG4B	BG5A	BG5B	BG6A	BG6B
Basket in	AE wsa	P,I	P,I	P,I	P,I	P,I,B	P,I	P,I	P,I	P,I												
	AE R15a	P,I	P,I	P,I	P,I	P,I,B	P,I	P,I	P,I	P,I												
	AE PZT																					
Basket out	AE wsa	P,I	P,I	P,I	P,I	P,I,B	P,I	P,I	P,I	P,I	I	I	I	I	I	I						I
	AE R15a	P,I	P,I	P,I	P,I	P,I,B	P,I	P,I	P,I	P,I	I	I	I	I	I	I						I
	AE PZT										I	I		I			I					

		T series				TF series				R series			S series			Basket	
		T1	T2	T3	T4	TF1	TF2	TF3	TF4	R1	R2	R3	S1	S2	S3	Top	
Basket in	Surface excitation																
	Surface sweeps																
Basket out	Passive basket sensing	I		I											I		
	BG excitation	F		F		F		F									
	BG sweep excitation	S															
	Surface excitation																
	Surface sweeps																
	Tone burst tuning	T															

		SG series									BG series											
		SG1	SG2	SG3	SG4	SG5	SG6	SG7	SG8	SG9	BG1A	BG1B	BG2A	BG2B	BG3A	BG3B	BG4A	BG4B	BG5A	BG5B	BG6A	BG6B
Basket in	Surface excitation					F																
	Surface sweeps					S																
Basket out	Passive basket sensing																					
	BG excitation																					
	BG sweep excitation																					
	Surface excitation					F																
	Surface sweeps					S																
	Tone burst tuning																					

Table 3.3: PWAS receiving and excitation locations

3.3.3 Results

To better understand the basic structural response of the small-scale dry cask mockup, various excitation methods were used: impacting balls, PLB and stainless-steel impacting. Frequency analysis via Fourier transform were used to examine these responses.

All the impacting balls of different diameters had very similar frequency response (Figure 3.9). The R15 α resonant type sensor produced a large resonance peak at 50 kHz and a small peak at the sensor's own resonance peak at 150 kHz. As expected the WS α wide band sensor produced more peaks but surprisingly produced no peaks after roughly 120 kHz.

Among the PLB tests results the R15 α signal contained three resonance peaks, where the largest fell at 150 kHz while the two smaller peaks appeared at approximately 50 kHz and 275 kHz (Figure 3.9). The WS α produced a much wider range of frequency components with many different peaks. The largest of which occurred slightly over 100 kHz.

The impact hammer produced significantly lower frequency components than those of the other methods. Peaks for both AE sensors fell under 200 kHz with no higher harmonics (Figure 3.9). The R15 α and WS α maximum peaks occurred at approximately 50 kHz and 20 kHz respectively.

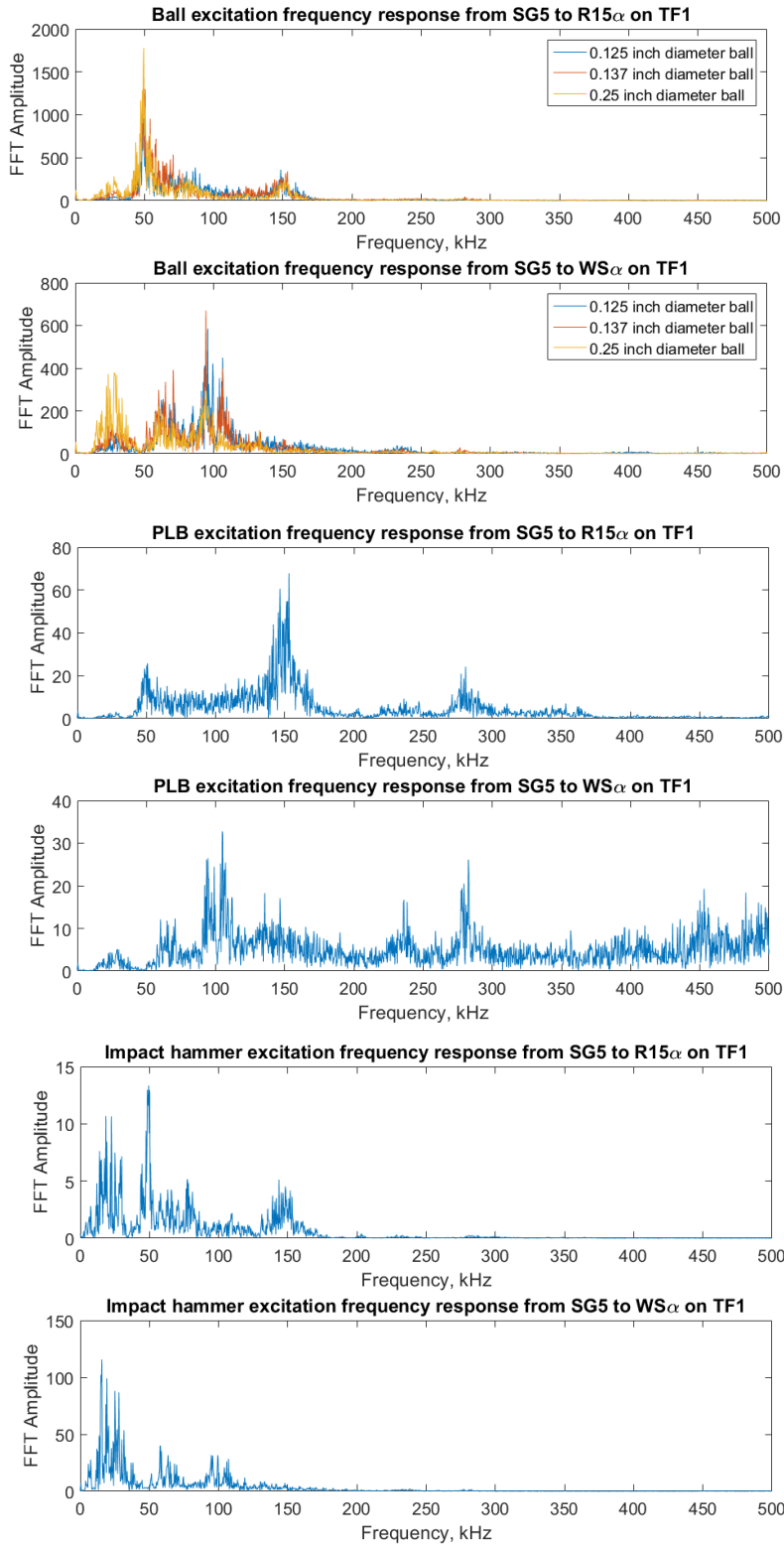


Figure 3.9: Shows the frequency domain of various excitation methods and sensor combinations

3.3.3.1 AE source localization

After configurations through replaying the AE events and tuning the parameters for optimal results, the AE source localization test via impact hammer and PLB were conducted. This was done by AEwin software integrated with the AE Micro II system by selecting the results in the localization graph and copying the calculated results from the data lookup display window. They were then moved to and plotted in MATLAB.

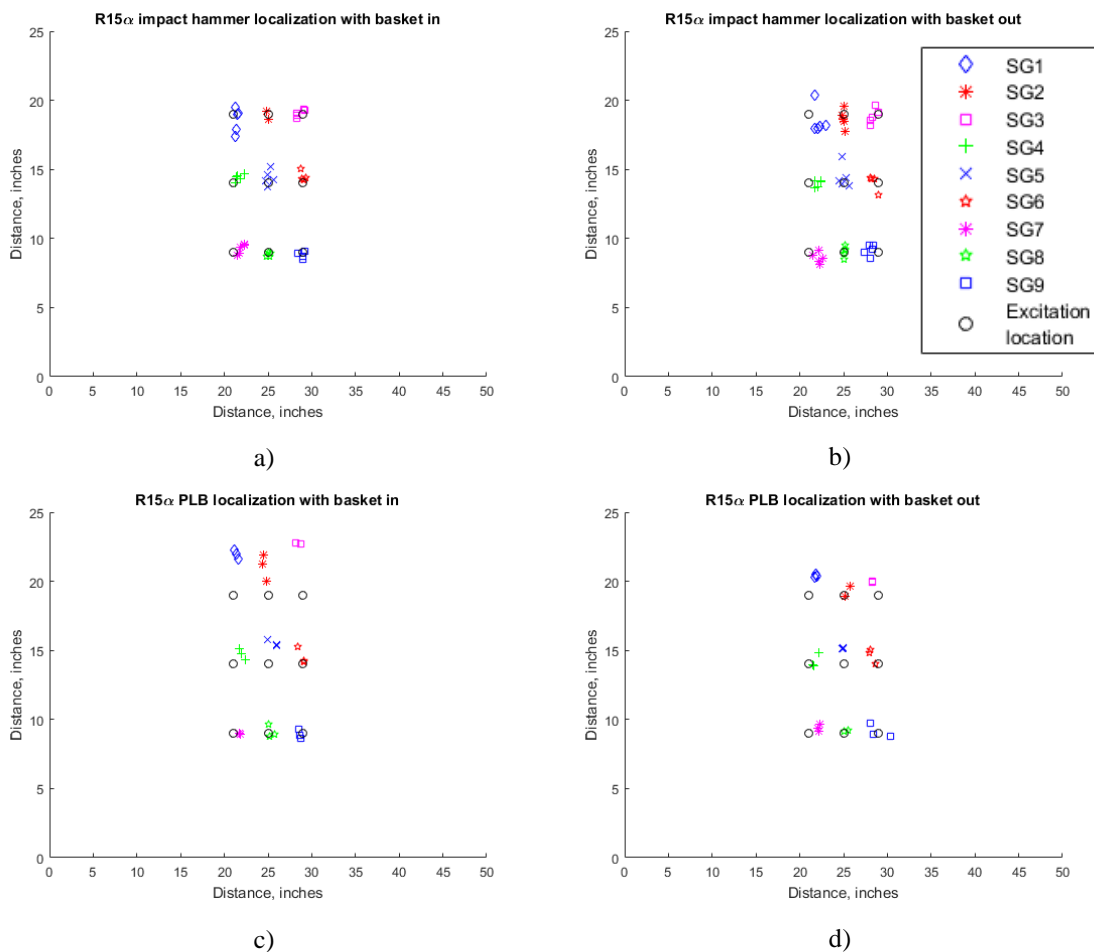


Figure 3.10: PLB and T304 tip impact hammer localizations of SG series using R15α

The R15α resonant type sensor results were first examined (Figure 3.10). All impacts were successfully detected and localized. The results were accurate where most

of the detected hits lay within an inch or two of the actual impact. The PLB with the basket out resulted in the least accurate calculated impact locations. The basket condition seemed to have negligible effect on the localization accuracy. Next the $WS\alpha$ wideband sensor data was analyzed (Figure 3.11).

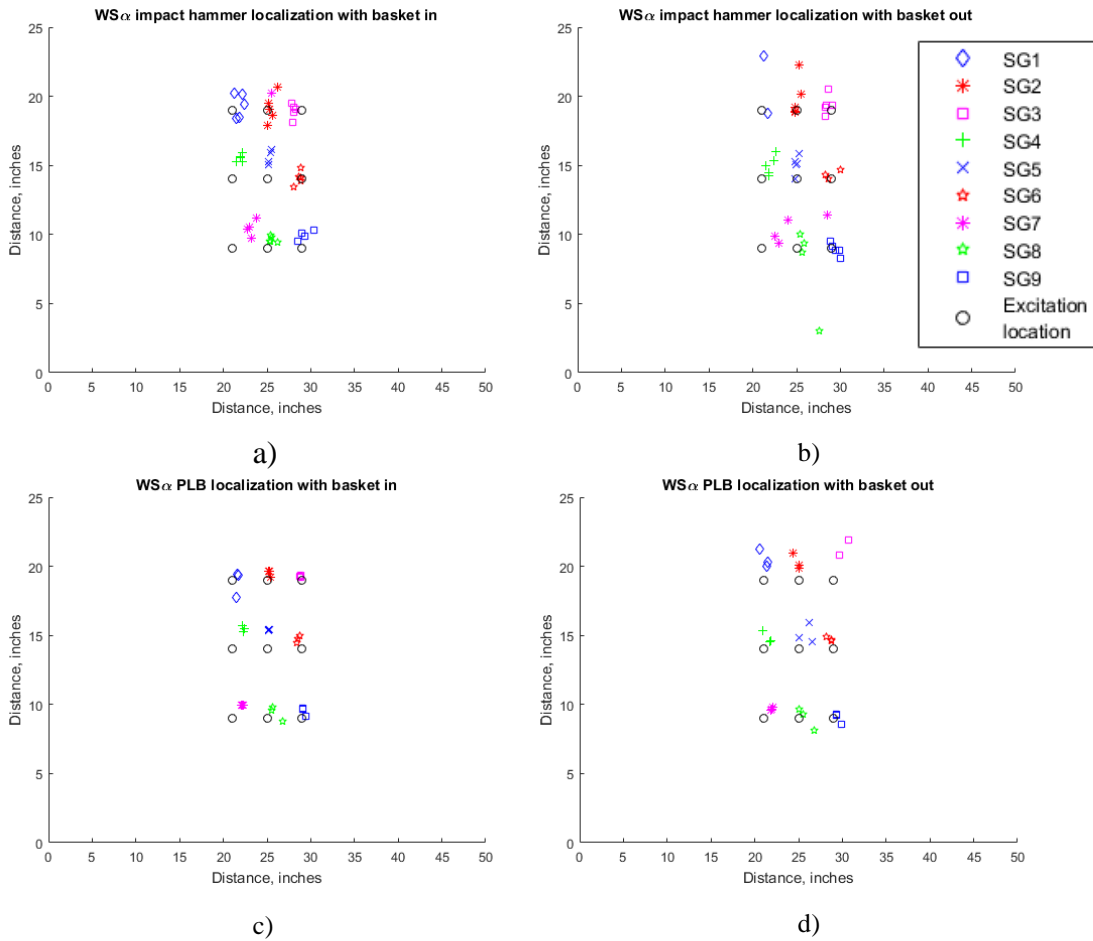


Figure 3.11: PLB and T304 tip impact hammer localizations of SG series using $WS\alpha$

Not all hits resulted in correct localizations. Some impacts were detected indeed outside of the structure and were ignored. The PLB localizations were similar to that of the impact hammer excitation.

Overall, of the detected localizations the $WS\alpha$ sensors produced less accurate results, however still within an inch of the excitation point. The wideband sensors seemed

more prone to miss or produce unreliable detections. Further study needs to be performed to understand the reason.

3.4 Full-scale AE tests

Building on the experiences acquired from medium and small-scale tests, field tests on full-scale representative dry storage cask were conducted. Procedures, methods and AE sensors used in the small-scale mockup were adopted to the full-scaled cask, except the carbon ball excitation method. Both passive and active sensing techniques were explored for the potential of integrated acousto-ultrasonic SHM/NDE for dry storage cask in the long run.

3.4.1 AE source localization tests

Localization techniques were explored on a full-scale dry storage cask using four R15 α AE sensors. Each sensor had a Physical Acoustic 2/4/6 preamplifier and was accompanied by the supporting AEwin software. Two experiments were conducted on a local region on the cask surface and on the entire surface of the cask, respectively.

3.4.1.1 localization on small area

The small region was a 3×4 feet square section on the surface of the cask (Figure 3.12). Blue painters tape was used to cover the impact surface. Locations labeled as A1, B1, C1, and D1 marked the placement of the AE sensors. The numbers represent the impact locations for an “a” series of AE. The “a” series contained 12 locations for impact localization. The coordinates were contained within a grid where the coordinates were determined as if the structure was a plane if the back of the cask was figuratively split

and the lower left corner was the origin. The one-inch shift within the “a” series grid was applied to avoid a welded seam.

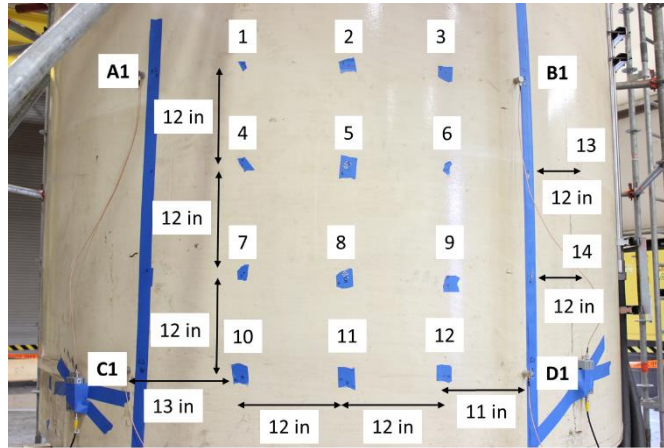


Figure 3.12: Impact locations on the front face consisting of the “a” series of excitation locations [30]

Five AE events were created for each location using the custom stainless-steel tip impact hammer used in previous small-scale test (Figure 3.13). For proper source localization a few test hits were performed first to determine appropriate calculation parameters. The preamplifiers operated at 20 dB; and the acquisition settings within AEwin were given in Table 3.4. After testing, the sensor locations were added within the AEwin software and the saved data could be “replayed” with different localization settings to localize the events (Figure 3.14). The wave speed and other parameters for localization were eventually estimated by trial and error (Table 3.5). The software also interprets the surface as planar, therefore the top and lower portion of the cask was ignored. Also, the settings are set such:

Table 3.4: Acquisition setup within AEwin for Experiment 1 where sensors A, B, C, and D were represented as 1, 2, 3, and 4 respectively

AE Channel	Threshold			Gain dB	Pre-Amp dB	Analog Filter		Waveform Setup		
	Type	dB	FTBnd			Lower	Upper	Sample Rate	Pre-Trigger	Length
<input checked="" type="checkbox"/> 1	FIXED	50	6	0	20	1kHz	3MHz	1MSPS	256.0000	5k
<input checked="" type="checkbox"/> 2	FIXED	50	6	0	20	1kHz	3MHz	1MSPS	256.0000	5k
<input checked="" type="checkbox"/> 3	FIXED	50	6	0	20	1kHz	3MHz	1MSPS	256.0000	5k
<input checked="" type="checkbox"/> 4	FIXED	50	6	0	20	1kHz	3MHz	1MSPS	256.0000	5k

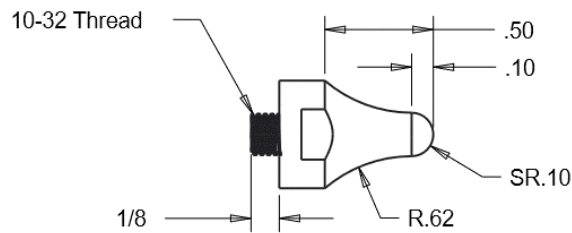


Figure 3.13: Impact hammer tip used for all experiments in inches [30]

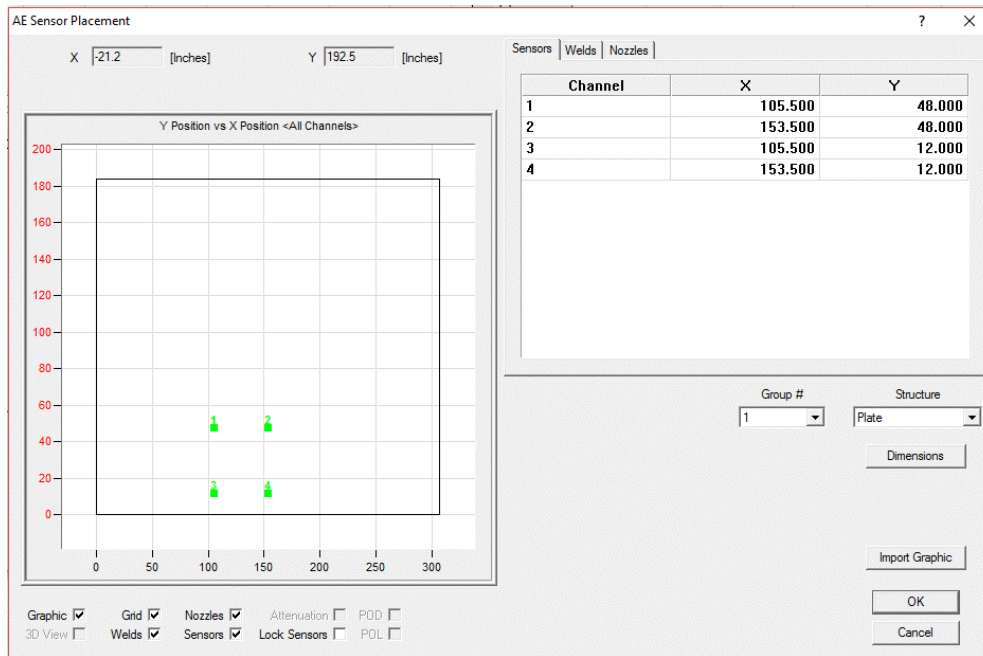


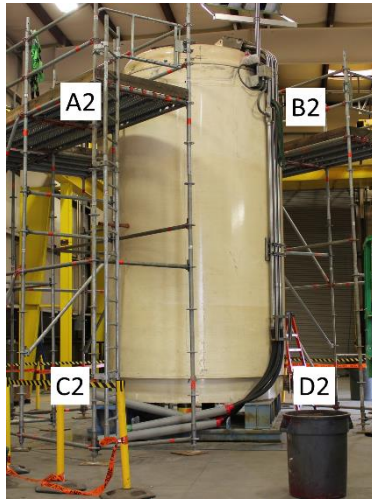
Figure 3.14: Sensor placement view for Experiment 1 [30]

Table 3.5: Localization setup for Experiment 1

Group #	Show All Points	Location Type	Wave Velocity	Event Definition Value	Event Lockout Value	Overall Value	Timing Strategies	Hits/Event		Max Iterations
								Min	Max	
<input checked="" type="checkbox"/> 1	<input checked="" type="checkbox"/>	2D Planar (XY)	215000.00	40.0000	0.0000	0.0000	Primary	3	5	256

3.4.1.2 Localization on whole structure

Following the first experiment the sensors were transferred and re-bonded to the trunnions. Each trunnion had a sensor and their locations labeled A2, B2, C2, and D2 (Figure 3.15a). The sensors were bonded halfway between the inner and outer portion of the trunnion (Figure 3.15b). Sensors were placed on the lower sections of trunnions A2 and B2, and the upper portion of C2 and D2.



a)



b)

Figure 3.15: Sensors moved to a) trunnions A, B, C, D with b) a close-up image of a bonded sensor on trunnion C [30]

New impacting points were determined (Figure 3.16) and locations recorded. New painter's tape was applied and marked during the process. The new impacting area consisted of 8 impacting locations. The coordinates were that of the previous method.

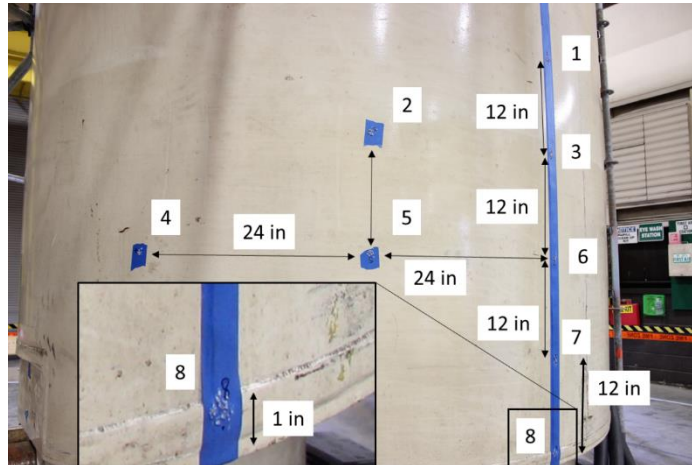


Figure 3.16: Layout of “b” series of excitation locations [30]

The same settings were used as in the previous full-scale sensing except for the preamplifiers and event definition value. The preamplification was increased to 40 dB for the larger area. The event definition value was increased to 110, otherwise many of the impacts would not be detected.

3.4.1.3 Results of small and large area localization

Following each setup simulated AE events were created, and waveforms recorded. For each test, 5 AE events were made with each being separated by a few seconds. After the data was collected and processed by in the AEwin software, the localization results were plotted in MATLAB. It is seen that the small area localization provided the better results as the estimated AE events fell within a few inches of the actual points (Figure 3.17). The accuracy decreased the farther along the horizontal axis the excitation point was located at. This effect occurred again on the large-scale localization but with the detected locations being within a foot in the excitation points (Figure 3.18).

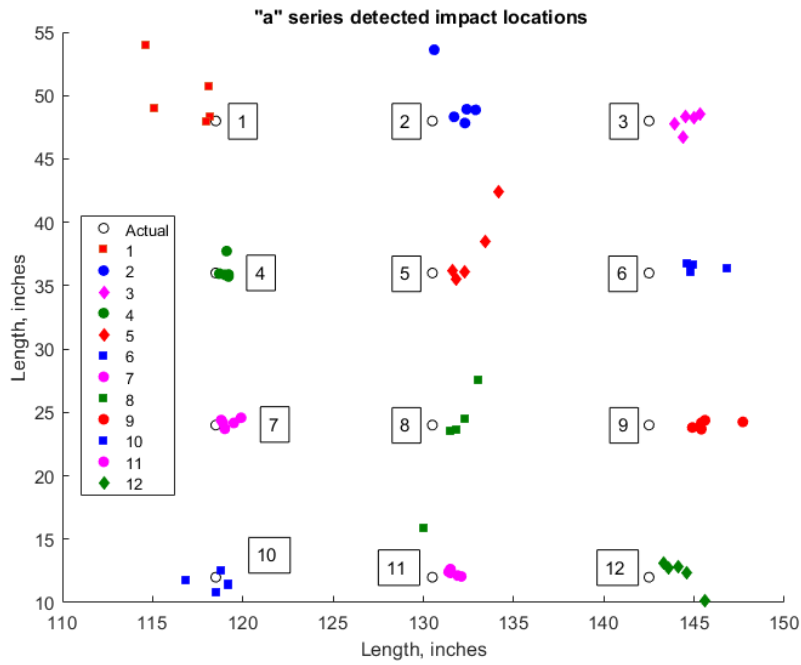


Figure 3.17: Series "a" detected impacts along with the actual locations [30]

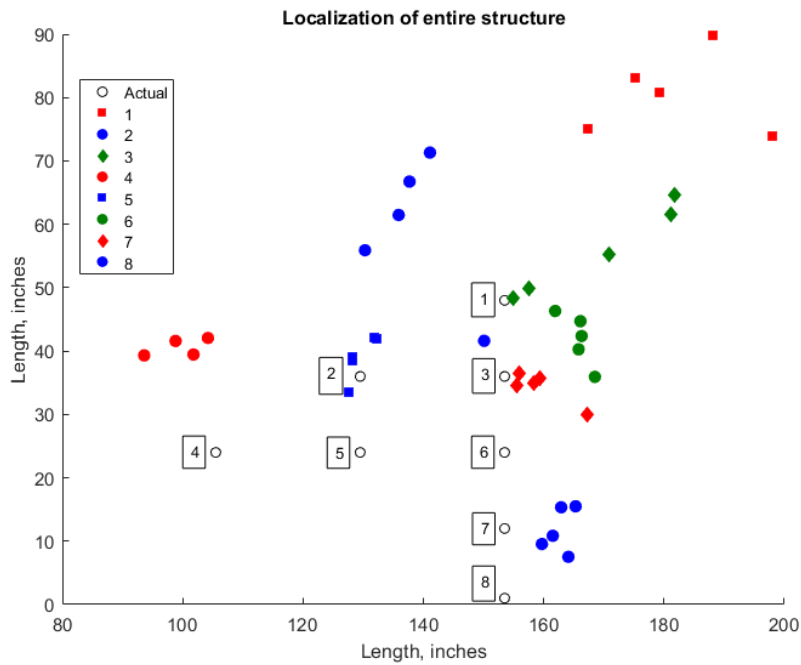


Figure 3.18: Series "b" of simulated AE locations and true locations [30]

3.5 Additional active sensing

Active sensing was carried out on the small- and full-scaled structures. However, when reviewing the data, it appeared that the bandpass filters used with the PWAS filtered out the structural response. Instead what was collected was more likely the PWAS and bonding response due to the thickness of the material. These higher frequency characteristics were both seen on the small- (Figure 3.19) and full-scale (Figure 3.20) frequency domain and amplitude plots. The plots exhibited a strong frequency component at 350 kHz which is uncharacteristic of large structures.

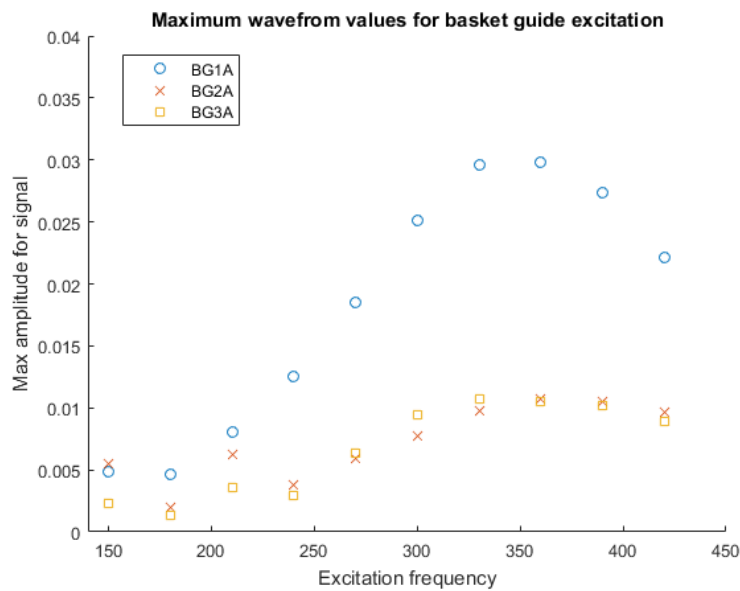


Figure 3.19: Small-scale max amplitude response measured from basket guides

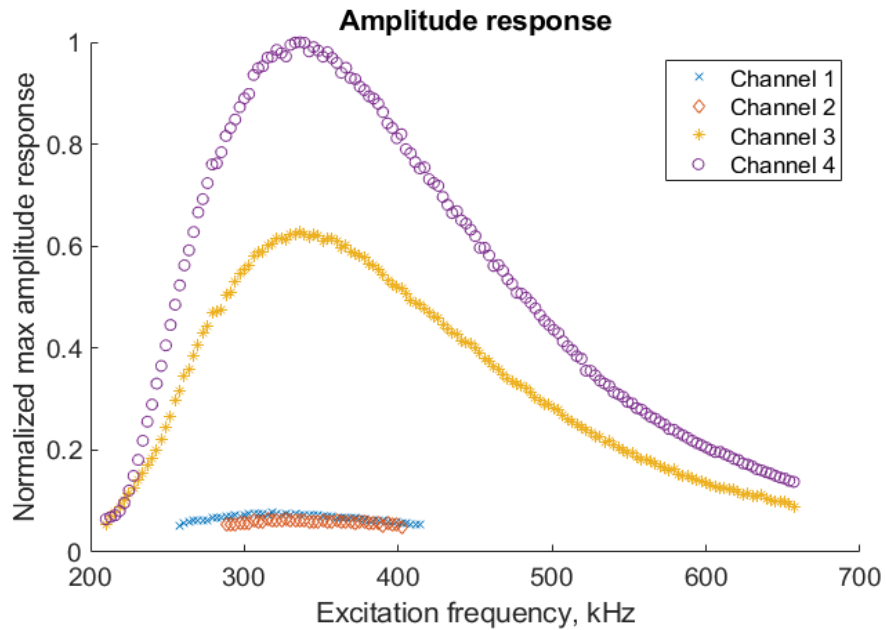


Figure 3.20: Full-scale max amplitude response with excitation frequency ± 6 kHz excitation error where the channels correspond with the trunnions [30]

3.6 Conclusions

Experiments were carried out on various nuclear structures or similar. Sensing capabilities using AE techniques were first explored on a medium-scale vacuum drying chamber. After which small-scale testing was conducted. Finally, active and passive experiments were conducted on a full-scale nuclear storage cask.

The medium-scale nuclear structure, excitation and sensing methods were examined. Testing showed that of the AE sensors used the R15 α and WS α performed best and were used in the later testing. The poor results of the R15i excluded it from continuing testing. The PLB produced the best signal to noise signal when compared to the impact hammer excitation. The plastic tipped impact hammer excitation was very poor in amplitude and was retired from future testing.

Applying the sensing techniques performed in the previous testing, research was carried out on the small scale dry cask. The field experiments gave a detailed look into the excitation and response of a small-scale mockup dry storage cask. Resonant and wideband passive AE sensors and passive and active PZT wafers were used in detecting responses created from many different sources. Localization was performed and resulted in excellent results as the estimated locations were near the excitation.

Full-scale testing was performed using passive and active means similarly to that of the small-scale testing. Using PWAS and AE sensors along with a variety of excitation methods, a detailed examination of ultrasonic methods was completed. Passive experiments yielded the sensing capabilities of excitation methods and sensor combinations as well as localization performance. Of the localization studies two experiments were carried out: a front face localization and of the entire structure. The front face produced excellent results as many of the estimated impact locations fell within inches of the actual occurrence. The full-scale localization produced good results, considering the size of the canister and sensor position, as many of the hits fell within a few feet. The active experiments on the full-scale cask were used to examine PWAS actuation and receiving. However, it appeared that important waveform information was likely lost because of a band pass filter on the preamplifiers.

CHAPTER 4 BOND QUALITY DETECTION

4.1 Introduction of bond layer contamination in composites

4.1.1 Problem definition

As aircraft technology progresses so does the number of composites used in the aerospace construction. The Boeing 787 uses more composites than any other Boeing ever made. Roughly 50% of the 787 aircraft's construction is composite [23]. With the greater use of composite materials comes the need of determining their health. Bonded composite structures, represents one of these needs [24]. Bonded structures are of interest as they offer the ability of combining dissimilar materials as well as more uniform stress distribution [24]. Bond quality evaluation is considered essential in determining flaws that could potentially reduce the health of these components.

Product defects in composites come in many different varieties such as voids, delaminations, contaminations, resin starved areas, resin rich areas, blisters, wrinkles, thermal decomposition and more [24]. Efforts to determine these damages through non-destructive evaluation are sought after using methods such as impedance-based, acoustic emission, and elastic-wave-based means [3]. Interest in elastic-wave-based techniques using non-contact methods of ultrasonic wave propagation has grown [3] and if investigated could potentially result in quick quality inspection systems.

4.1.2 Scope of this work

Within this chapter various sensing methods that have shown their potentials in composite structures NDE will be examined with respect to their applications toward bond quality inspection. To obtain this goal, first bonded specimens will be fabricated for experimentation. Contact bond quality evaluation will then be conducted using impedance based and then traditional immersion tank C-scan methods. After these, a non-contact inspection system will be developed and evaluated with regards to sensitivity, functionality, and versatility. The non-contact inspection system will be assembled from sensors, computers, and necessary hardware/devices to provide automatic scanning ability over a given region. Finally, the non-contact system will be used to detect defects and bonding contaminations. The contact and non-contact methods will be compared and sensing capabilities of the systems will be evaluated.

4.2 Specimen preparation

Five bonded specimens that host delaminations, weak bonds, voids, and adhesive addition were created for experimentation.

4.2.1 Materials for bonded specimens

To insure realistic testing, plate materials had to be chosen. Two types of plate materials were considered in this study: the aluminum and carbon fiber reinforced polymer (CFRP) composite; with the former being well-understood isotropic material to study the sensing methodologies themselves and the latter being typical composites being used in aero structures for the targeted bond quality study. The aluminum plates used were 2024-T3 of 0.063 inch thickness. The composite plates were 8-ply (0, 45, 90, 135)s

with a thickness of 0.100 inches made of 34-600 fibers and NCT 301-1. 3M AF 555 adhesive film was available and has been used by other researchers for bonding composite plates, and hence was selected for the bonding.

The aluminum plates did not need any special processing before the bonding procedure. For composite plates, before bonding they were placed inside of a sealed box along with four silica gel packs to remove any moisture within. Before bonding the adhesive film was removed from an -10°F freezer and was cut to an oversized plate length. These were placed in a sealed box so that condensation would not build on the surfaces of the adhesive. The time the adhesive was removed and allowed to warm was recorded (Table 4.1).

Table 4.1: Bonded specimens made and their characteristics with approximate warming time

Specimen	Material	Size, in	Damage type	Warming time, hr
1	2024-T3	18×18	Weak bonding	22.75
2	2024-T3	12×12	Weak bonding	43.75
3	2024-T3	12×12	Delamination, voids, additions	47.75
4	Composite	12×12	Weak bonding	22.5
5	Composite	12×12	Weak bonding	28.5

4.2.2 Heat press bonding process

To begin the bonding of both aluminum and composite plates, debris was removed from the non-mating surfaces. Then Teflease MG2 PTFE high temperature tape was applied to the non-mating surface close to the edges. This tape would allow for cured adhesive spilled on the surface of the plates to be easily removed. The plates were then flipped over where surface preparation began. A Wabash heat press was used to bond the

plates. All specimens bonded were placed in between Wrightlon 8400 bagging film to prevent the specimens sticking to the machine. A single recipe was used (Table 4.2).

Table 4.2: Recipe 1 used for all specimen bonding

Segment	Temperature, F	Pressure, tons	Time, minutes	Function
1	0-355	0.2	65	Increase temperature
2	355	0.2	120	Hold temperature
3	355-111	0.2	30	Cool off

4.2.3 Surface preparation

To ensure the quality of bonds being made, a careful process was followed such that the plate surfaces to be bonded together were properly prepared. The bonding surface preparations for aluminum and composite slightly vary. The aluminum specimen preparation used a combination of wet sanding with phosphoric acid and cleaning with neutralizer. For the composite specimens denatured alcohol was used for wet sanding and later again for cleaning.

4.2.4 Damage creation within specimens

After the surfaces were prepped, various defects were introduced to the specimens for simulating “defects”. Damages created include weak bonds (from contamination) [18], delamination, void, and damage accumulation. These methods were used on both the aluminum and composite specimens.

4.2.4.1 Weak bonding due to contamination

For specimens 1, 2, 4 and 5 (composite and aluminum), weak bonds were created by introducing various contaminants that were applied to the bottom portion of the top plate. This was done to form three bonding conditions within the bonded plates (Figure

4.1). Two types of contaminations were used in this study: silicone oil and Frekote. Silicone oil and Frekote were chosen as both are present within industry and pose a potential risk of being introduced during bonding. Once within the adhesion layer NDE of the strength or properties of the bond has proven difficult to determine [31].

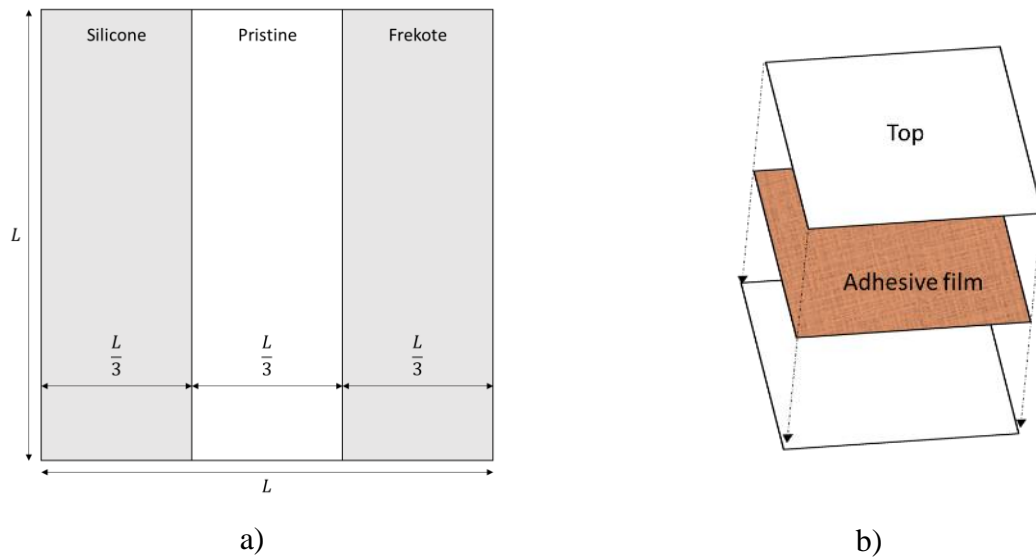


Figure 4.1: Plate damage layout from Specimens 1, 2, 4, and 5 from a) top down view and b) layup view

Tape was used to make three distinctive different bonding regions (Figure 4.2a). Frekote was applied to a medical gauze and then wiped on the right portion of the plate. Silicone spray was applied to a clean gauze and wiped on the left portion of plate. After which the tape was removed and the plate was allowed to dry for approximately 5-10 minutes (Figure 4.2b).

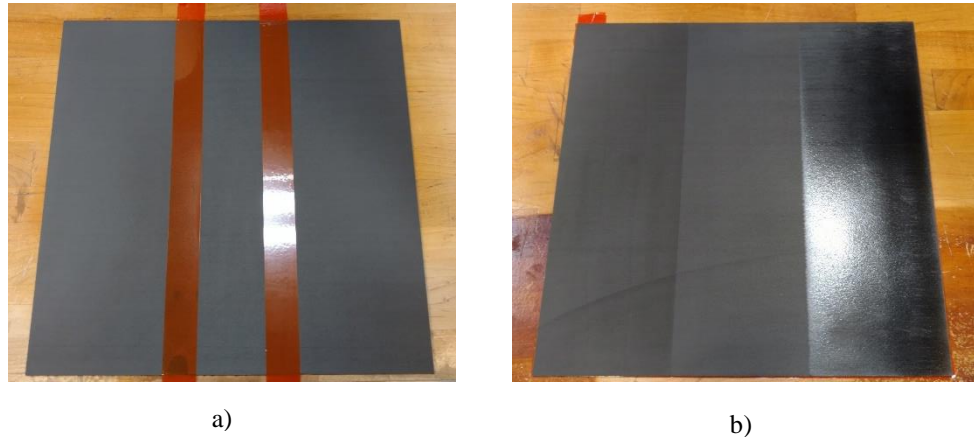


Figure 4.2: Process of weak bonding a) before application of contaminates and b) after drying for a composite specimen

On the mating surface of the other plate, the room temperature film adhesive had one side of protective film removed and was placed on the prepared surface. The air bubbles were removed, and excess material cut off (Figure 4.3).



Figure 4.3: Adhesive film applied to non-contaminated side and being cut

Next the secondary protected film was removed and the top plate flipped (so that the contaminates were facing down), set on top of adhesive, and had the plate corners precisely aligned. Then the plates were placed between bagging film and set inside of the Wabash heat press where they followed Recipe 1 (Table 4.2).

4.2.4.2 Delamination, voids, and additional material defects bonding

Specimen 3 consists of delaminations, voids, and adhesive addition within the bonded plates. To create the delaminations bagging film was cut into 1 inch and 0.5 inch squares and a strip that measures roughly 3.25 inches long and 0.25 wide (Figure 4.4a). These pieces of bagging film were placed on top of the bottom plate. Adhesive film was then carefully laid on top of the surface of the plate so that the film would not move. The void was created by removing a 1 inch by 1 inch square section with a razor blade from the adhesive film. This was done while one layer of protective film remained adhered to prevent unintentional contamination. After cutting, the film was removed and a 1 inch square placed on the opposite side on top of the adhesive for an adhesive addition defect (Figure 4.4b). The overall arrangement of the damages are shown in Figure 4.5a, as well as the layup view (Figure 4.5b). After the preparation, the top plate was added and the entire assembly was placed between bagging film inside of the heat press where they followed Recipe 1 (Table 4.2).

Now the specimens are ready for the study of evaluating the bond quality. Both contact type (using electromechanical impedance method and ultrasonic C-scan) and non-contact type (using air-coupled transducers and/or scanning laser Doppler vibrometer) were to be performed and given in the subsequent sections.

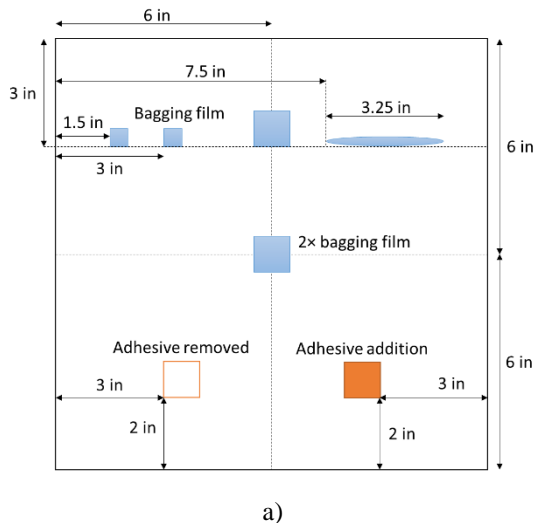


a)

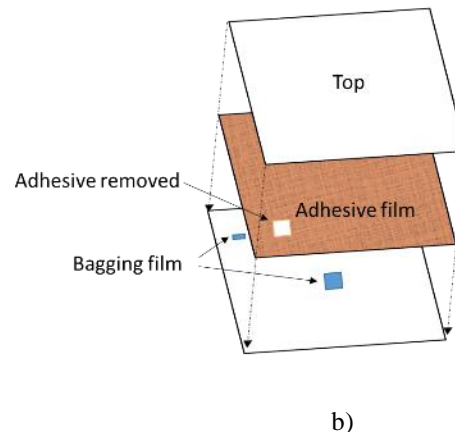


b)

Figure 4.4: Damage preparation of Specimen 3 with a) prepared bagging tape sections to be inserted in and b) plate with adhesive applied where a section is removed to create a void



a)



b)

Figure 4.5: Specimen 3 a) damage layout and b) layout were locations of bagging film can be seen

4.3 Impedance method

4.3.1 Preparation

Plate 2 was selected for impedance testing to investigate the bond quality through well-established contact means. With PWAS bonded to the surface of the plate the

impedance of the structure was measured through its electro-mechanical coupling [4]. After cleaning and sanding surface preparation, 18 PWAS were bonded to front surface of the plate in three grids of six sensors to get the impedance at different locations of the bonded regions (Figure 4.6). The sensors were labeled from 1 to 18 starting from the top left most sensor, progressing to the right in a descending manner after each row.

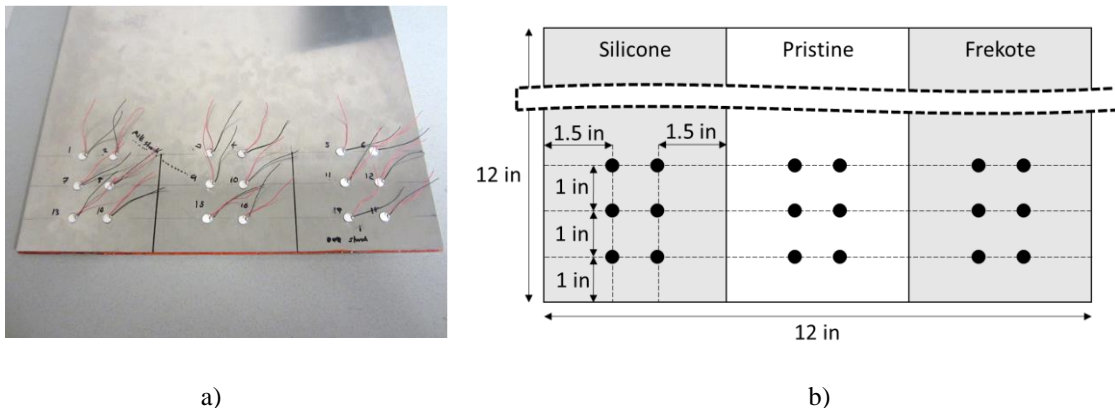


Figure 4.6: Plate 2 with a) sensors attached and b) layout of sensors

4.3.2 Procedure

To acquire the impedance of the structure a HP 4194 A impedance analyzer was used and connected to the bonded PWAS. The impedance was first measured from 40 kHz to 1000 kHz at 1 kHz steps for the in-plane peaks; and then 4000 to 6000 kHz at 1 kHz steps for the through-thickness peaks. The data was recorded and the impedance spectral data were compared to the various bonding conditions.

4.3.3 Results

The points measured for the impedance based comparison was the first and through-thickness mode peaks observed in the impedance spectrum. Examples of the peaks from Point 1 are shown in Figure 4.7. For the acquired spectra, it has been found

their first peaks occurred approximately 360 to 460 kHz while the through-thickness peaks fell within the 4.5 to 5 MHz range.

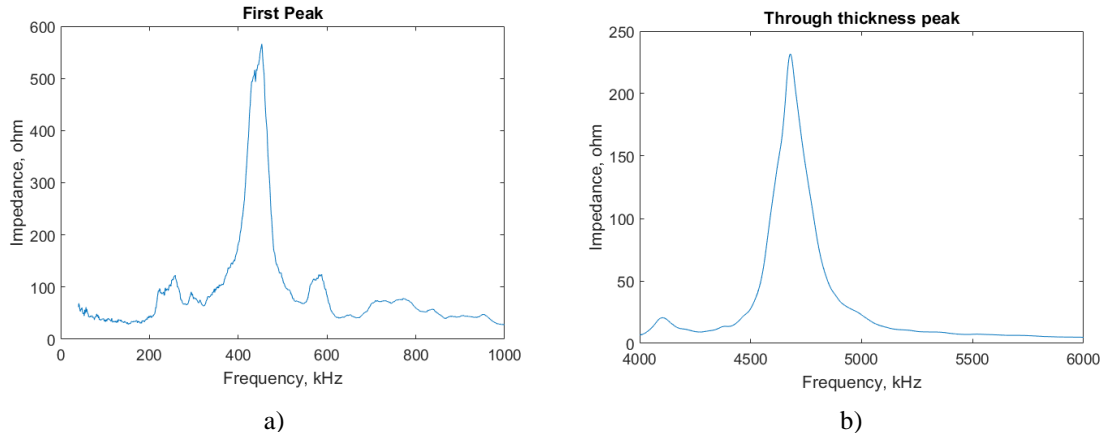


Figure 4.7: Sample data from Point 1 of a) first peak resonance and b) through thickness resonance

The maximum values from the first peak and through thickness mode peaks along with their corresponding frequencies were then collected and plotted to observe any trends that could indicate any variation of bond quality for different cases (Figure 4.8). However, from the results that have been achieved in this study, no differences between the pristine areas and either contaminated regions can be observed. The peak values showed no indication of change within the bond layer. In addition, the pristine bonded results were significantly more scattered.

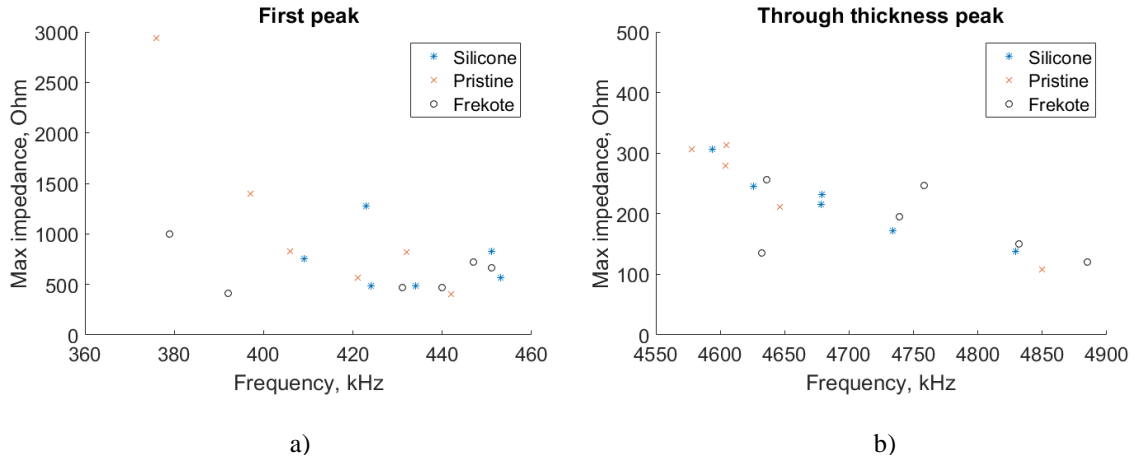


Figure 4.8: Max impedance resonance and their corresponding frequencies at a) first peak and b) through thickness peaks

4.4 Immersion tank C-Scan

Ultrasonic C-scans using immersion tank is standardized NDE for defect evaluation. Hence an immersion tank test was also prepared for bond quality evaluation to see if any could be detected.



Figure 4.9: Immersion tank used for ultrasonic C-scan inspection

4.4.1 Preparation

The tank (Figure 4.9) was filled with tap water and metal blocks were arranged on the floor of the tank so that they would support the edges of the plate under inspection. The blocks would be shifted once a specimen of different size was used.

4.4.2 Procedure

To scan the specimens, the software package ODIS was used to operate the motion controllers as well a data acquisition. Low resolution test runs were first made to align the plate to be inspected. After which, the data was collected and MATLAB used for further analysis.

4.4.3 Results

After immersion tank scanning on all specimens was completed and it turned out that certain defects and contaminations could be identified. As expected the immersion tank easily detected all delamination and the adhesive voids and addition were identifiable (Specimen 3). Also observed was the interesting adhesive bonding pattern along the edges of the plate, likely due to changes of heat and pressure during bonding. Some bond layer contamination could also be seen on the aluminum specimens (specimens 1 and 2). When examining various time settings for the C-scan, the Frekote contamination appeared through most of the absolute peak amplitude (APA) windowed signal. However, the silicone contamination seemed to be undetectable on the aluminum plates (Figure 4.10).

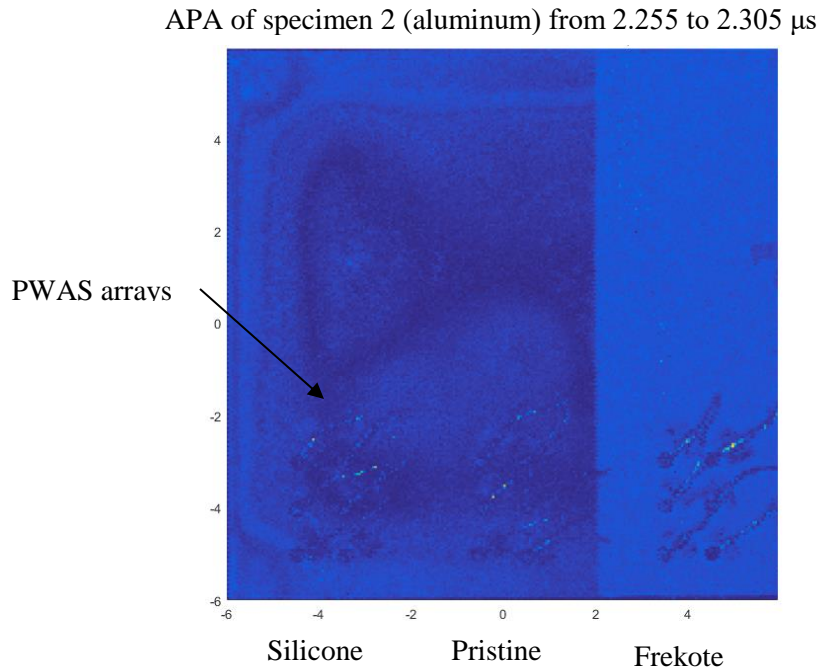


Figure 4.10: Immersion tank scan of Specimen 2 using a 10 MHz focused transducer using pulse echo single penetration displaying APA of signal between 1.235 to 1.285 μ s

During the immersion tank scan of the composite plate Specimen 5, factory plate defects were identified inside of the specimen (Figure 4.11). Unfortunately, no silicone or Frekote contamination defects were detected. Observing the arrival time of the signals acquired in factory defects area, it indicates that the damage was within the top layers of the plate. When examining the surface of the plate, the damage could be seen with the naked eye. A second closer immersion scan was completed (Figure 4.11 call out) to examine the details and later to be compared with the results of the non-contact system.

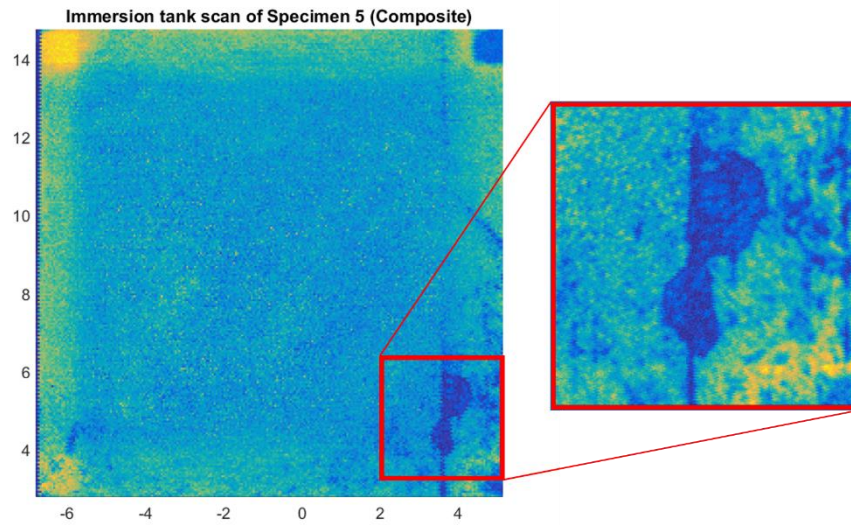


Figure 4.11: Immersion tank scan of Specimen 5 using a 10 MHz focused transducer pulse echo single penetration displaying APA of signal between 1.73 to 1.78 μ s with closeup of 3 \times 3 inch area of selected damaged area

Specimen 4 was scanned with the immersion tank and the silicon or Frekote contamination was not detected either. The damages were determined to possibly come from two similar flaws in two separate plates that created a “X” pattern when bonded. This was to be used for the comparison of various methods later in the conclusions (Figure 4.21).

4.5 Non-contact scanning systems

Non-contact ultrasonic sensing through air coupled transducers (ACT) and/or laser Doppler vibrometry (LDV) have also been explored with in this study to evaluate the bond quality. The system used here consists of various devices and equipment that can acquire sensing data to be later processed with additional software; while accommodating interchangeable excitation and acquisition methods.

4.5.1 Non-contact sensing and scanning system development

4.5.1.1 System overview

The system's main components consist of a computer, a 3-axis CNC machine, an acquisition system, and an oscilloscope. The 3-axis machine moves the affixed actuator and/or sensor in 3 directions (x-y-z) over the desired inspection area. It is automatically controlled by ODIS software in the computer, as well as the acquisition system and the oscilloscope (Figure 4.12). Note the oscilloscope was not necessary but used for troubleshooting and special-purpose data acquisition cases. To excite and acquire the signals for the ACTs, Airscan hardware will be used. The system will collect the ultrasonic signals and then export them into MATLAB for further data analysis.

In addition, manual scanning and oscilloscope data acquisition can also be used to complete the ultrasonic sensing when the LDV is selected as the sensor; but the process is quite lengthy (roughly 1.8 minutes per measurement point) limited by current hardware setups.

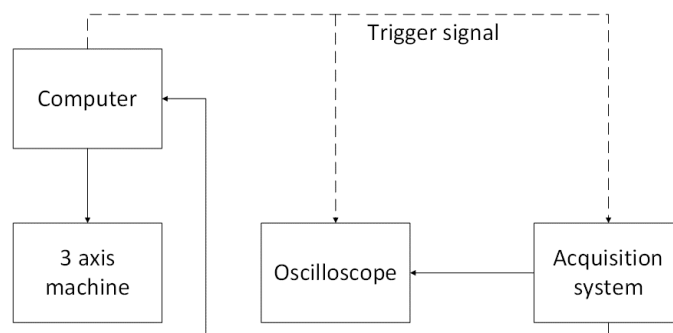


Figure 4.12: Simple block diagram of the system

4.5.1.2 Sensor combination and position

The sensing acquisition systems can consist of either ACT and ACT (ACT-ACT) or ACT and LDV (ACT-LDV) to implement non-contact ultrasonic C-scan techniques in a similar manner to the traditional immersion tank. The ACT transducers used in this study operate at 120, 225, or 400 kHz resonant frequencies. Various locations on the specimens were scanned and inspected using one of the combinations given above.

To perform ultrasonic C-scan, the selected sensors (ACT or LDV) were aligned in the same Z axis for through transmission sensing (Figure 4.13). For the ACT actuators, they were positioned at the manufacturer's recommended distance of 1.2 inches (30 mm) normal to surface of the plate. They remained fixed while the specimen was moved by the 3-axis machine for the scanning of the desired area. During the scanning process, the specimen remained normal to the actuators and sensors.

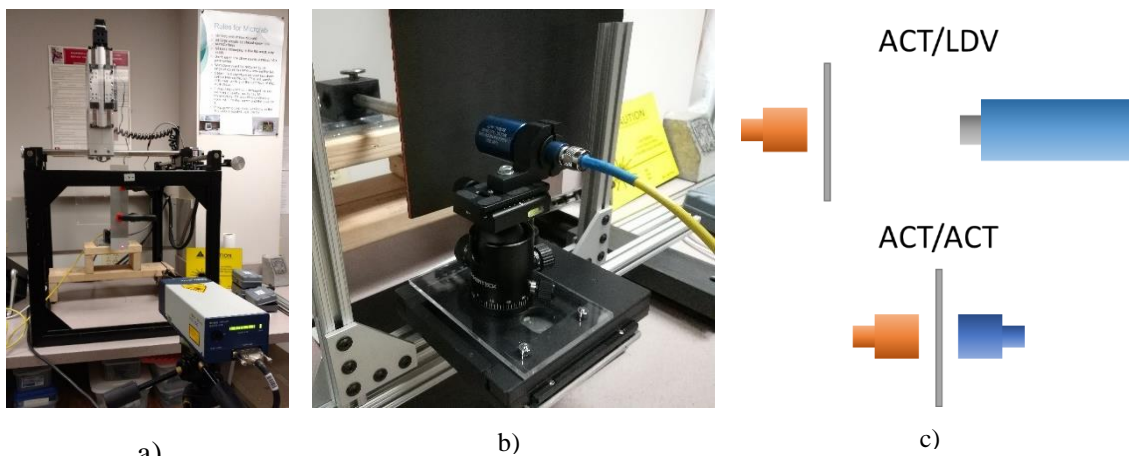


Figure 4.13: The scanning system a) equipped with ACT-LDV, b) ACT-ACT and c) diagram of sensor alignment

4.5.2 Procedure

To properly operate the ACT system, the trigger signal needed to be inverted since the Airscan system uses a falling edge while the trigger signal in the ODIS system

needs a rising edge. An inverter chip was implemented to invert the trigger signal. The ACT actuator was tuned to produce the maximum signal to noise ratio following the Airscan user manual. Variables include the transducer resonant frequency, actuation, tuning, and cycles. Once the ACT system was turned on, ODIS was then used to scan without averaging due to the current limitation of ODIS (it would crash if performing averaging). The collected data was saved in MATLAB data format.

For ACT-LDV configuration, the LDV distance to the plate was set at two feet. However, preliminary study found that the ACT excited ultrasonic waves were too weak to be properly collected using the LDV if averaging was not used. Hence, instead of using ODIS system, the oscilloscope was used for the ACT-LDV setup. The oscilloscope was set to collect data at a sampling rate of 10 MHz with a 10 k record length. For the ACT-ACT configuration, ODIS was used for data acquisition.

4.5.3 Results

The ACT-ACT scanning system produced intensity images where the X and Y axis indicate locations in the plate and the colors represent the absolute peak amplitude of the measured ultrasonic signals at the locations. The scan area dimensions were made to a 1:1 aspect ratio. Depending on the location being scanned, the scanning increments would change accordingly to accommodate the size of the scan area and the scanning time. For the bond layer inspection, the non-contact system would be compared to immersions tank scans.

4.5.3.1 Bagging film detection

Before bond layer inspection, detection of bagging film induced disbonds inside Specimen 3 (aluminum) was preformed to explore the ACT-ACT system's capabilities. Scan areas of interest on the specimen for inspection were identified (Table 4.3). These scan areas are indicated in Figure 4.14 using red boxes. A large area scan was also selected and performed to include all Locations 1, 2, 3, and 4.

Table 4.3: Scan parameters

Scan location	Area size, inches	Scan increment, inches	Surf plot grid size
Location 1 and 2	1×1	0.01	1010×1000
Location 3	1.5×1.5	0.01	1010×1000
Location 4	3.5×0.5	0.02	1760×250
Large area scan	11×1.5	0.05	2110×300

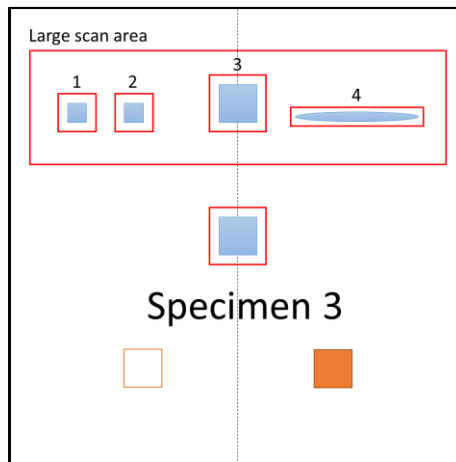


Figure 4.14: Scan areas on Specimen 3

All Specimen 3 scan results were given by the absolute peak amplitude of the entire signal (APA). The Large areas scans were made first using ACT transducers at 120, 225, and 400 kHz frequencies. After the Large scan areas are processed, a closer look at the individual locations was conducted. Location 1 was viewed first (Figure 4.15).

Observation of the images showed an interesting phenomenon. The 120kHz and 225 kHz ACT-ACT sensors resulted in the damage having a higher amplitude (Figure 4.15a and b). However, when using the 400 kHz transducers the resulted of the damaged regions showed a lower amplitude. Due to the time-consuming process, only a single ACT-LDV scan was completed (Figure 4.15d).

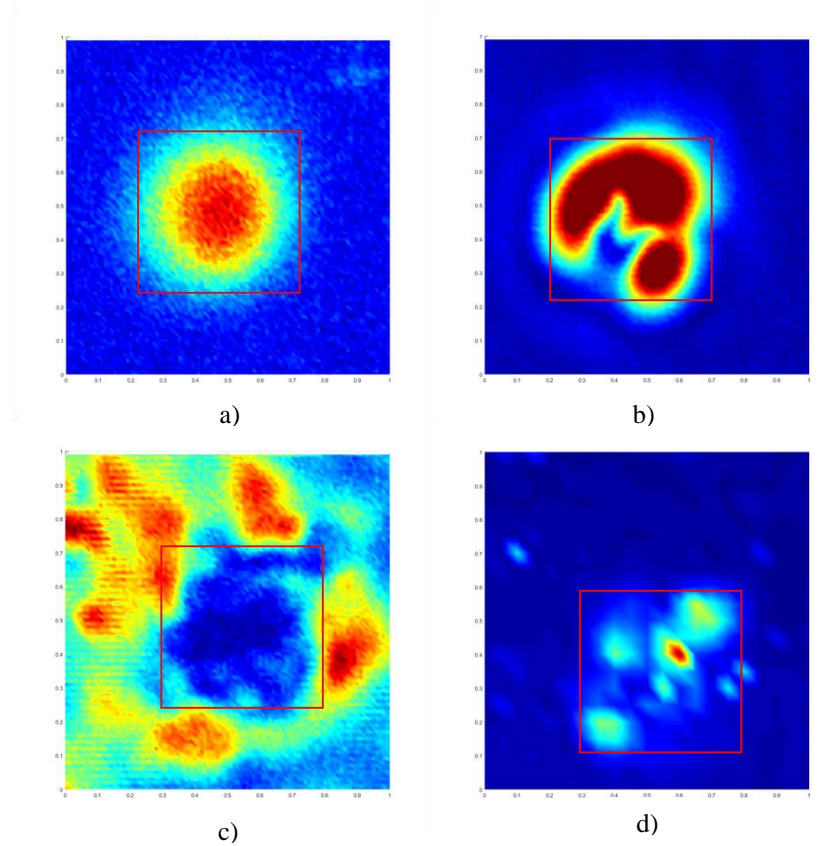


Figure 4.15: Location 1 APA scan area detecting a 0.5 by 0.5 inch bagging film using a) ACT-ACT at 120 kHz Settings 1 b) ACT-ACT at 225 kHz c) ACT-ACT at 400 kHz d) ACT-LDV at 225 kHz where the red box indicates the disbond size and location

Further testing with the ACT-ACT system showed consistent results between the different locations on Specimen 3. On locations 1, 2, and 3 it appeared that even though the damage was detected the images created by the 120 kHz were “fuzzy,” and more difficult to identify the damage. This worsened at Location 4 (Figure 4.16). The delamination strip ends contained the highest amplitude with the 225 kHz transducers but

seems to miss the rest of the bagging film. The 400 kHz scan resulted in the full damage being seen. The film was nearly undetected with the 120 kHz transducers.

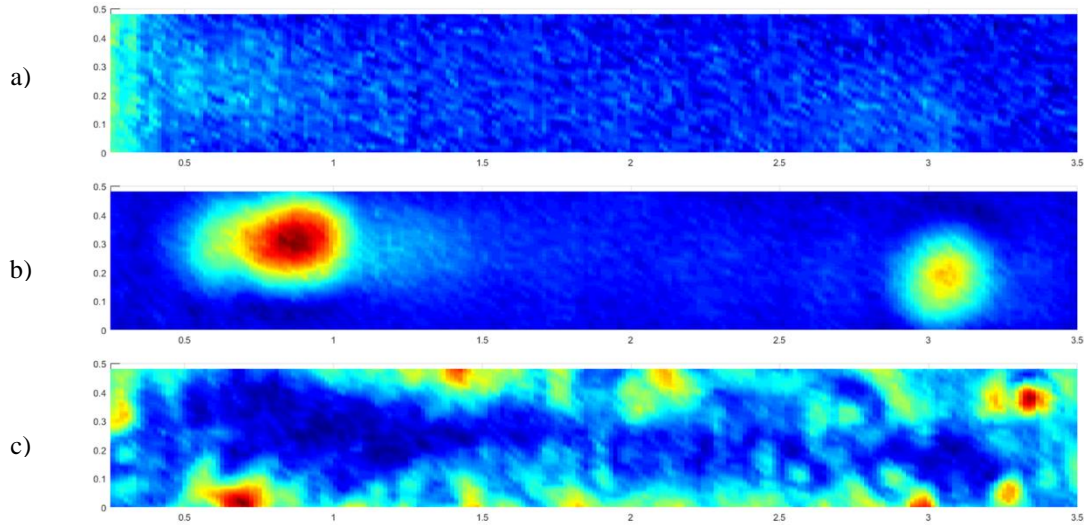


Figure 4.16: Location 4 APA scan area detecting a roughly 3.25 by 0.25 inch section of bagging film using a) ACT-ACT at 120 kHz b) ACT-ACT at 225 kHz c) ACT-ACT at 400 kHz

4.5.3.2 Bond layer inspection

Non-contact ACT-ACT bond quality inspection was performed using 120 kHz, 225 kHz, and 400 kHz. The aluminum specimens were first examined. The Frekote damage was easily identified by all frequencies (Figure 41). Again, the silicone contamination was not detected. When comparing all the contact and non-contact methods, the details observed in the 400 kHz ACT-ACT scan was comparable to that seen in the immersion C-scan.

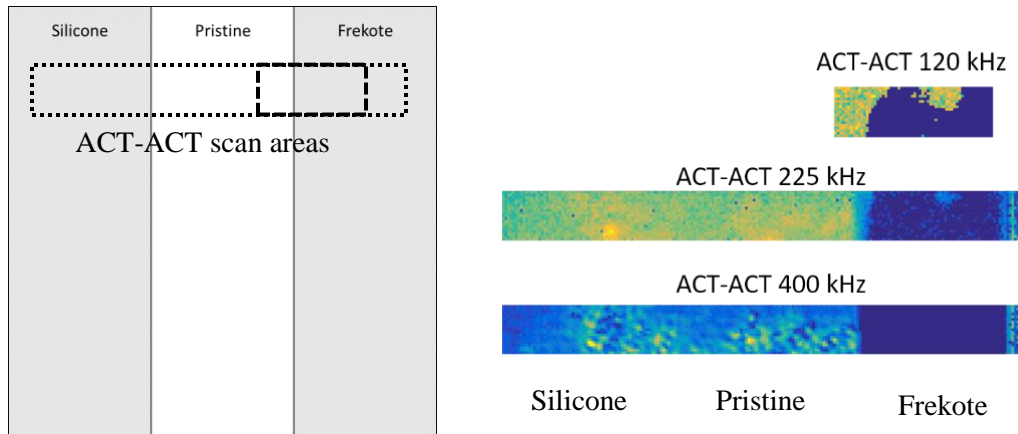


Figure 4.17: ACT-ACT 120, 225, and 400 kHz 2× APA a) scan areas and b) scans

When examining the composite specimens all transducers of the ACT-ACT system could detect the factory defects. The 400 kHz ACT-ACT scan produced the best resolution, however, with the least contrast between the damage and pristine areas. This was due to the lower signal to noise ratio. Unfortunately, no bond layer contaminations were detected.

4.6 Problems encountered

4.6.1 Software

The acquisition software ODIS seemed to be the main difficulty in scanning as the length of line scanning was limited. If the line consists of too many points the software will crash. Sometimes the motor controls would not respond requiring a software or computer reboot. Also, at the beginning of some scans the motors would perform odd maneuvers, moving the specimen a few inches. If not careful, could drive the plate into the scanning frame.

The most significant drawback was the faulty averaging tool as the average settings did not properly average the signal. If the secondary averaging settings were

adjusted within the scan parameters, the program would abort before scanning. This means the weak ACT-LDV signals were unable properly create images without averaging. Hence requiring lengthy and tedious manual scans.

4.6.2 ACT-ACT Excitation frequency

After much of the data was gathered using the ACT-ACT system the signals examined appeared that the noise in front of the signal might be reflections from within the plate. Lower transmission frequencies could be used to examine this part of the signal.

4.6.3 Specimen design

During experimentation the composite specimens were difficult for sensing. This was likely due to the thickness of the specimens. If the thickness was decreased could result in added sensitivity of the methods used.

4.7 Preliminary studies

The research within this section was focused on this supplementary study. Details of PL principles and applications are not the focuses of this thesis.

4.7.1 Robotic actuation

The current practice in the lab has actuators either being fixed or attached to the 3-axis gantry system. To allow for more flexible movement of the transducers, preliminary study on designing a robotic fixture to move actuator using a PL as a testing device was accomplished.

4.7.1.1 Robotic movement implementation

Mounting the actuator (pulse laser) on a robotic arm would be a solution to achieve the flexible and controllable movement and therefore increase the excitation capabilities of PL actuation system. KUKA KR6 robotic arm has been identified and selected to implement the motion control in this study. To mount the laser on the KUKA KR6 robotic arm an adaptor plate was needed. Since a real PL is not necessarily needed for teaching the robot desired motions, a dummy laser was made with the same dimensions and weight as the actual PL in the lab (Quantel CFR 400).

4.7.1.2 PL dummy

The PL dummy was built from a wooden block and fitted with an iron core to simulate the weight. The block was supplied with a Class 1 laser and external leads to power it. Once mounted using the adaptor plate (Figure 4.18), procedures could be practiced for future experiments.



a)



b)

Figure 4.18: Dummy pulse laser a) flange and b) mounted on a KUKA KR6

4.7.1.3 Function box

The KUKA computer through the EtherCAT (ethernet for control automation technology) can communicate with outside instruments. In the case of the PL excitation

in the non-contact system a trigger signal is needed to synchronize the instruments. This signal could be made within the KUKA programming and via BECKOFF controllers can be relayed as a high or low digital value. However, within the laboratory quick changes for averaging and excitation rate are desired and to make those changes within the KUKA software would be tedious and therefore a control box was built (Figure 4.19).

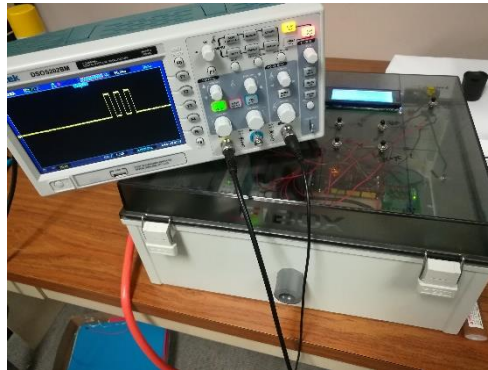


Figure 4.19: Function box with oscilloscope resting on top showing the output signal
This function box receives the 24 volt signal from the KUKA computer, indicating that the robot has positioned and through a microcontroller exports the desired averages and excitation rate trigger signal at 5 volts. These settings are displayed on a liquid crystal LCD.

4.7.2 PL alignment (For stationary PL excitation)

The pulsed laser needed means of determining the laser beam path. To accomplish this, two additional Class I line lasers were placed within two custom housings. These housings were threaded on top of optic table posts (Figure 4.20a). The lines from the crosshairs formed the beam path at their intersections. Calibration was required and custom targets were made to do so. Once bolted down range facing the PL on the same optic table, the surface of the target was painted with black erasable marker

and the pulsed laser fired. A single pulse would remove the paint in the laser beam, showing the exposed metal surface. The laser would be adjusted to the impact location and the line lasers would be in alignment.

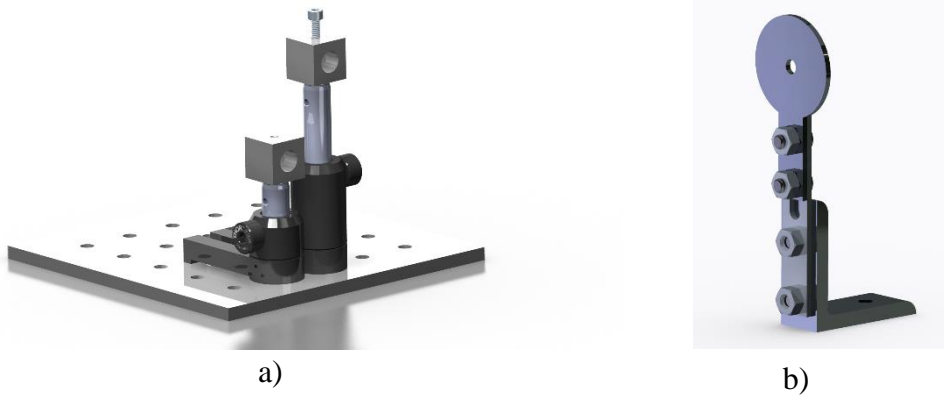


Figure 4.20: Alignment tools with a) line laser housings and b) target for calibration

4.8 Conclusions

Various methods using contact and non-contact means were explored on bonded specimens. Some methods proved more sensitive to damages than others. Impedance sensing techniques with piezoelectric wafers produce poor results as no correlation was seen in the results. The lack of sensitive was most likely related the small differences in sensor bonding as little variations could cause dramatic changes in the spectral measurements.

The ACT-LDV system was tedious to use but produced better results. The current software capability however limited the functionality of the system. The system performed poorly as the sensitivity of the laser was poor due to the low level of excitation produced by the ACT transducer. Even with the shortcomings a delamination was detected within the bond layer.

The ACT-ACT was an improvement of the other non-contact method. Scans produced interesting results where different transducers showed different trends. Using the 120 and 225 kHz transducers resulted in the amplitudes of the delaminated damaged regions being higher than the pristine areas in the APA C-scans. This changed once the 400 kHz was used. As expected, the definition of the delaminated areas improved as the frequency increased. When used to identify bonding contaminations, all the ACT-ACT transducers could find the Frekote contamination within the bond layer of the aluminum specimens. However, the silicone contamination remained undetected. When examining the composite plates, the specimens were found to have many factory defects which all were detected by the ACT transducers. When examining the bond layer within the composite specimens the contaminations were undetected.

Overall immersion tank scanning performed the best compared to the nonconventional methods (Table 4.4). ACT-ACT techniques were the most comparable as it detected all that the immersion tank could, however at slightly lower detailed level. Close examination of the ACT-ACT and immersion C-Scans shows the similarities between the two methods (Figure 4.21 and Figure 4.22).

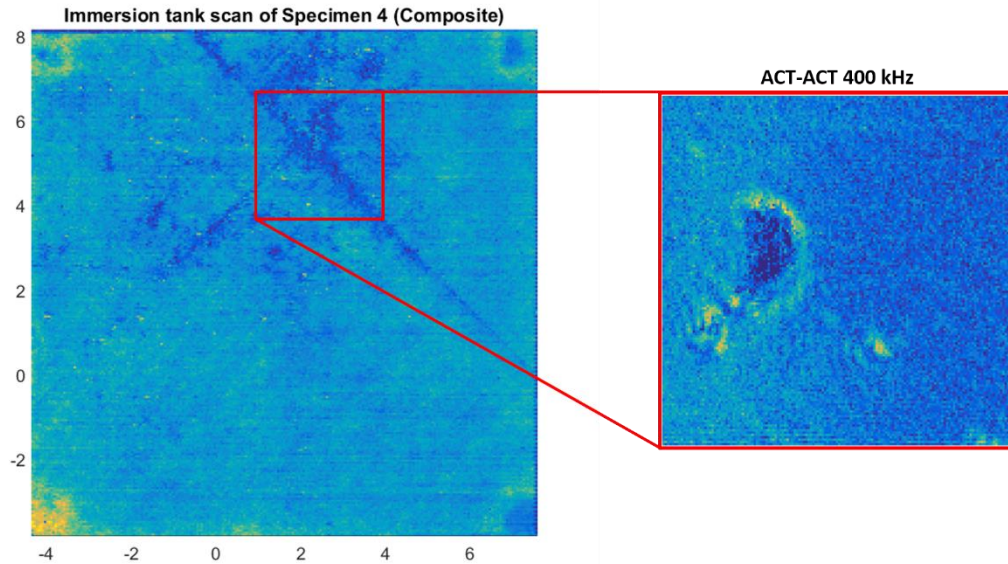


Figure 4.21: Immersion tank scan of Specimen 4 APA between 1.575 and 1.625 μ s at with closeup of ACT-ACT 400 kHz scan APA between 300 and 301 μ s

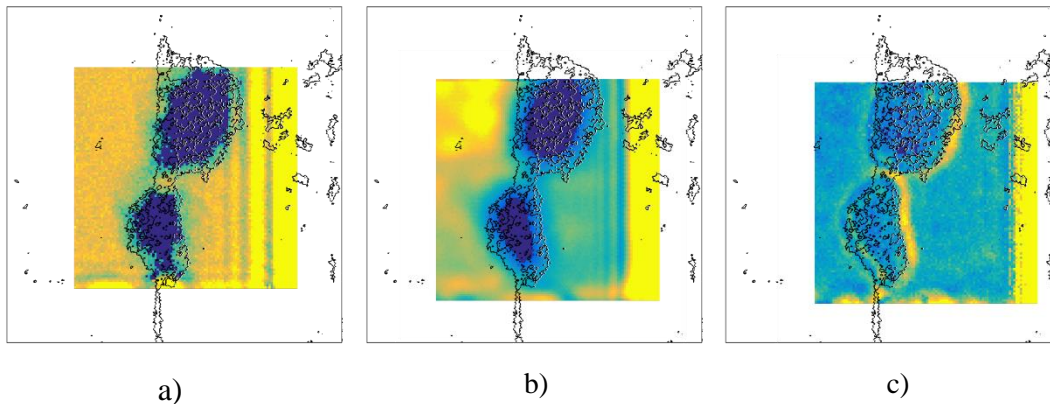


Figure 4.22: ACT-ACT 2x2 inch through transmission APA 50 to 100 μ s C-Scan of damage on Specimen 4 of damaged region with 3x3 inch immersion scan contour overlap using a) 120 kHz b) 225 kHz and c) 400 kHz transducers

Though mixed results were produced does not draw absolute conclusions on the usefulness of the methods used (Table 4.4). The specimens experimented on were thick and therefore more difficult to detect small differences. Techniques used may have resulted in more detailed results if implemented on thinner structures. Even with these

difficulties, damages and bond layer contamination were identified on the aluminum specimens using non-contact means.

Table 4.4: Systems used and abilities to detect bond layer damages in specimens tested

Sensing method	Aluminum Frekote contamination	Aluminum silicone contamination	Composite Frekote contamination	Composite silicone contamination	Detailed manufacturing defects	Manufacturing defects
Immersion tank	✓				✓	✓
ACT-ACT	✓					✓
ACT-LDV						✓
Impedance						

CHAPTER 5 CONCLUSIONS

Ultrasonic NDE/SHM offers the potential for relatively affordable and effective sensing [3]. The ability to provide detailed analysis without damaging while continuously monitoring a structure makes those methods very attractive. This thesis explored and applied several sensing techniques to evaluate the sensing capabilities of ultrasonic NDE/SHM for nuclear and aerospace structures applications.

For the nuclear dry storage cask health monitoring, AE sensors were first applied to determine AE sensing capabilities on a medium-scale complex vacuum drying chamber. After establishing the sensing range and AE behaviors, the preferable excitation as well as AE sensor types were selected and carried to small- and large-scale testing. On the small-scale cask mock-up, active sensing using similar hardware was also explored in addition to the AE methods. Response characteristics from multiple excitation methods in many difference structural conditions were acquired and analyzed. This included AE source localization which produced acceptable results as the detected hit events fell within a few inches of the source. The small-scale study guided the testing methods for tests to be done on full-scale cask as well as providing details on sensing parameters and settings. Following the small-scale experiments, full-scale cask NDE was executed using the same methods and procedure. A significant volume of data was collected from the field experiments that included passive AE sensing and structural response studies. Localizations were performed on the full-scale cask which produced excellent results considering the size of the structure. Of the localization for simulated AE events on the

front surface of the cask, the error was within inches, while for the entire cask within a few feet of the actual locations. Overall, the work completed on the dry storage casks SHM lead to the publications of three conference papers [29, 30, 32] and the better understanding of AE sensing on real dry storage casks. Future efforts can be focused on exploring other embeddable sensors such as fiber Bragg grating (FBG) sensors that can be installed on the cask structure during manufacturing stage to perform life-long monitoring and damage detection. Another interesting topic to continue our exploration can be the development of high-temperature piezoelectric sensors for nuclear power plant health monitoring applications.

The sensing and evaluation of bonded structures in aerospace applications focused on exploring non-contact ultrasonic NDE/SHM methods through comparison to traditional contact methods. Experiments with primarily non-contact ACT transducers were performed to detect silicone and Frekote contaminations within bonded composite and aluminum specimens. The achieved C-scan results were then compared to the traditional contact-type C-scan using immersion scanning. The Frekote was detected in both the ACT-ACT and immersion scanning within the bonded aluminum specimens. The Frekote was however undetectable in the bonded composite specimens but certain factory produced defects were identified. Silicone contamination remained undetected in all specimens. An impedance contact method was also attempted but failed to detect any conditions. This was likely due to the subtle differences in bonding. Even with these mixed results we still build the knowledge of bond layer contamination and the findings of the experiments were passed along to assist in future research. Continuing research would involve robotic NDE. Through fully non-contact means various techniques could

be used for bond layer investigation of complex shaped composite components. Advanced analysis methods such as nonlinear models could be explored for more detailed investigation. Through improved software higher resolution images could also be made. With more tools the effectiveness of noncontact ultrasonic NDE bond layer contamination could be better established.

REFERENCES

- [1] Wikipedia, "Aloha Airlines Flight 243," 16 May 2018. [Online]. Available:
https://en.wikipedia.org/wiki/Aloha_Airlines_Flight_243.
- [2] Federal Aviation Administration, "Aircraft Accident Report," FAA, 1989.
- [3] Z. Su and L. Ye, Identification of Damage Using, Springer, 2009.
- [4] V. Giurgiutiu, Structural Health Monitoring with Piezoelectric Wafer Active Sensors, Oxford: Elsevier, 2014.
- [5] Quality Material Inspection, "Airscan," 2017. [Online]. Available:
<https://www.qmi-inc.com/airscan.php>.
- [6] Polytec, "NON-CONTACT VIBRATION MEASUREMENT," 2018. [Online].
Available: <https://www.polytec.com/us/vibrometry/>.
- [7] R. U. Naoki Hosoya, A. Kanda, I. Kajiwara and A. Yoshinaga, "Lamb wave generation using nanosecond laser ablation to detect damage," *Journal of Vibration and Control*, 2017.
- [8] A. J. Duncan, P.-S. Lam, R. L. Sindelar and J. T. Carter, "Crack Growth Rate

Testing With Instrumented Bolt-Load Compact Tension Specimens Under Chloride-Induced Stress Corrosion Cracking Conditions in Spent Nuclear Fuel Canisters," in *ASME Pressure Vessels and Piping Conference*, Waikoloa, Hawaii, 2017.

- [9] S. J. Vahaviolos, *Acoustic Emission: Standards and Technology Update*, West Conshohocken: American society for testing and materials, 1999.
- [10] Physical Acoustics, "Sensors," Mistras Group, 2018. [Online]. Available: <http://www.physicalacoustics.com/sensors/>.
- [11] U. S. N. R. Commission, "Dry Cask Storage," 22 August 2017. [Online]. Available: <https://www.nrc.gov/waste/spent-fuel-storage/dry-cask-storage.html>.
- [12] The National Academies of Sciences Engineering Medicine, "Safety and Security of Commercial Spent Nuclear Fuel Storage: Public Report," The National Academies Press, 2006.
- [13] World Nuclear Association, "Storage and Disposal of Radioactive Waste," July 2017.
[Online]. Available: <http://www.world-nuclear.org/information-library/nuclear-fuel-cycle/nuclear-wastes/storage-and-disposal-of-radioactive-waste.aspx>.
- [14] Holtec International, "HI-STAR 100," Holtec International, 2018. [Online]. Available: <https://holtecinternational.com/productsandservices/>

wasteandfuelmanagement/dry-cask-and-storage-transport/hi-star-3/hi-star-100/.

- [15] R. H. J. Jr., "Dry Storage Cask Inventory Assessment," U.S. Department of Energy, 2016.
- [16] O. Chopra, D. Diercks, D. Ma, V. Shan, S.-W. Tam, R. Fabian, Z. Han and Y. Liu, "Managing Aging Effects on Dry Cask Storage Systems for Extended Long-Term Storage and Transportation of Used Fuel," Argonne National Laboratory, 2013.
- [17] S. Chatzidakis, S. Cetiner, H. Santos-Villalobos, J. Jarrell and J. M. Scaglione, "Sensor Requirements for Detection and Characterization of Stress Corrosion Cracking in Welded Stainless Steel Canisters," 2018.
- [18] X. He, R. Benke, Y.-M. Pan, L. Caseres, P. Shukla, K. Chiang, R. Pabalan, G. Willden and D. Vickers, "Available Methods for Functional Monitoring of Dry Cask Storage Systems," U.S. Nuclear Regulatory Commission, 2014.
- [19] C. J. Lissenden, S. Choi, H. Cho, A. Motta, K. Gartig, X. Xiao, S. L. Berre, S. Brennan, K. Reichard, R. Leary, B. McNelly and I. Jovanovic, "Toward Robotic Inspection of Dry Storage Casks for Spent Nuclear Fuel," vol. 139, no. 031602-1, 2017.
- [20] C. Lissenden, S. Choi, H. Cho, A. T. Motta, K. Hartig, X. Xiao, S. L. Berre, R. Leary, B. P. J. Mcnelly and I. Jovanovic, "Robotic Inspection of Dry Storage Casks

- for Spent Nuclear Fuel," in *Pressure Vessels and Piping Conference*, 2016.
- [21] S. Chatzidakis, C. K. Choi and L. H. Tsoukalas, "Analysis of Spent Nuclear Fuel Imaging Using Multiple Coulomb Scattering of Cosmic Muons," *IEEE Nuclear and Plasma Sciences Society*, vol. 63, no. 6, 2016.
- [22] American Composite Manufacturers Association, "Composites vs. Aluminum," compositeslab, 2016. [Online]. Available: <http://compositeslab.com/composites-compared/composites-vs-aluminum/>.
- [23] The Boeing Company, "BOEING 787 FROM THE GROUND UP," 2008. [Online]. Available: http://www.boeing.com/commercial/aeromagazine/articles/qtr_4_06/article_04_1.html.
- [24] U.S. Department of Transportation Federal Aviation Administration, "Aviation Maintenance Technician Handbook - Airframe," 15 May 2014. [Online]. Available: https://www.faa.gov/regulations_policies/handbooks_manuals/aircraft/amt_airframe_handbook/.
- [25] Federal Aviation Administration, "Literature Review of Weak Adhesive Bond Fabrication and Nondestructive Inspection for Strength Measurement," U.S. Department of Transportation, 2015.
- [26] D. Sokol and D. Lanhrman, "Laser Bond Inspection (LBI)," in *A4A NDT*, 2014.

- [27] M. Perton, A. Blouin, J.-P. Monchalain and M. Arrigoni, "Adhesive bond testing by laser shock waves and laser interferometry," in *NRC*, 2010.
- [28] P. Malinowski, L. Skarbek, T. Wandowski and W. Ostachowicz, "CFRP Bonds Evaluation Using Piezoelectric Transducers," in *NDT in Aerospace*, 2012.
- [29] S. Howden, B. Lin, P.-S. Lam, T. Knight and L. Yu, "Health monitoring on medium scale structures using acoustic emission methods," in *International Congress on Advances in Nuclear Power Plants*, Charlotte, 2018.
- [30] S. Howden, B. Lin, L. Yu and V. Giurgiutiu, "Acoustic emission and active sensing capabilities on full-scale nuclear cask storage structures," in *SPIE Smart structures+ nondestructive evaluation*, Denver, 2018.
- [31] R. Ecault, B. Ehrhart, M. Boustie, C. Bockenheimer, B. Valeske, F. Touchard and L. Berthe, "Laser Adhesion Test for Adhesive Bonded CFRP Structures," *4th International Symposium on NDT in Aerospace*, 2012.
- [32] R. Joseph, S. Howden, B. Lin, L. Yu and V. Giurgiutiu, "Active health monitoring of TN32 dry cask using a scaled down model," in *SPIE*, Denver, 2018.
- [33] S. Howden, B. Lin, L. Yu and V. Giurgiutiu, "Acoustic emission and active sensing capabilities on small- and full-scale nuclear cask storage structures," in *SPIE Smart structures+ nondestructive evaluation*, Denver, 2018.